NAVAL POSTGRADUATE SCHOOL

MONTEREY, CALIFORNIA

THESIS

MODELING SCHOTTKY BARRIER GaAs SOLAR CELL USING SILVACO ATLAS

by

Steamboat Rock

June 2018

Thesis Advisor: Sherif N. Michael
Second Reader: Matthew A. Porter

THIS PAGE INTENTIONALLY LEFT BLANK

REPORT DOCUMENTATION PAGE			*Form Approved OMB No. 0704-0188*

1. AGENCY USE ONLY *(Leave blank)*	**2. REPORT DATE** June 2018	**3. REPORT TYPE AND DATES COVERED** Master's thesis

4. TITLE AND SUBTITLE MODELING SCHOTTKY BARRIER GaAs SOLAR CELL USING SILVACO ATLAS	**5. FUNDING NUMBERS** Solar
6. AUTHOR(S) Steamboat Rock	
7. PERFORMING ORGANIZATION NAME(S) AND ADDRESS(ES) Naval Postgraduate School Monterey, CA 93943-5000	**8. PERFORMING ORGANIZATION REPORT NUMBER**
9. SPONSORING / MONITORING AGENCY NAME(S) AND ADDRESS(ES) N/A	**10. SPONSORING / MONITORING AGENCY REPORT NUMBER**

11. SUPPLEMENTARY NOTES The views expressed in this thesis are those of the author and do not reflect the official policy or position of the Department of Defense or the U.S. Government.

12a. DISTRIBUTION / AVAILABILITY STATEMENT Approved for public release. Distribution is unlimited.	**12b. DISTRIBUTION CODE** A

13. ABSTRACT (maximum 200 words)

Gallium Arsenide (GaAs) solar cells are proven lightweight and high power density photovoltaic devices that offer significant performance improvements over conventional silicon solar cells; however, only a handful of commercial companies currently produce GaAs cells due to manufacturing costs. The objective of this thesis is to investigate the combined performance of several uncommonly used methods of fabricating thin-film GaAs solar cells, which show promise in reducing the cost of cell fabrication. Using Silvaco ATLAS Technology Computer Aided Design (TCAD), we simulated and optimized the performance of back-side contact thin-film solar cells. In such a design, both anode and cathode contacts are placed on the same side of a device, resulting in no shadowing of incoming light. The replacement of the AlGaAs emitter with a Schottky junction was simulated and evaluated and compared to the original back-side contact design. Finally, a method of improving the Schottky barrier height of the Schottky design was simulated and evaluated.

14. SUBJECT TERMS Single-junction, solar cell, SILVACO Atlas, optimization, simulation, modeling, photovoltaic	**15. NUMBER OF PAGES** 77
	16. PRICE CODE

17. SECURITY CLASSIFICATION OF REPORT Unclassified	**18. SECURITY CLASSIFICATION OF THIS PAGE** Unclassified	**19. SECURITY CLASSIFICATION OF ABSTRACT** Unclassified	**20. LIMITATION OF ABSTRACT** UU

NSN 7540-01-280-5500 Standard Form 298 (Rev. 2-89) Prescribed by ANSI Std. 239-18

THIS PAGE INTENTIONALLY LEFT BLANK

Approved for public release. Distribution is unlimited.

MODELING SCHOTTKY BARRIER GaAs SOLAR CELL USING SILVACO ATLAS

Steamboat Rock
Lieutenant, United States Navy
BS, North Carolina State University, 2008

Submitted in partial fulfillment of the
requirements for the degree of

MASTER OF SCIENCE IN ELECTRICAL ENGINEERING

from the

NAVAL POSTGRADUATE SCHOOL
June 2018

Approved by: Sherif N. Michael
Advisor

Matthew A. Porter
Second Reader

Clark Robertson
Chair, Department of Electrical and Computer Engineering

THIS PAGE INTENTIONALLY LEFT BLANK

ABSTRACT

Gallium Arsenide (GaAs) solar cells are proven lightweight and high power density photovoltaic devices that offer significant performance improvements over conventional silicon solar cells; however, only a handful of commercial companies currently produce GaAs cells due to manufacturing costs. The objective of this thesis is to investigate the combined performance of several uncommonly used methods of fabricating thin-film GaAs solar cells, which show promise in reducing the cost of cell fabrication. Using Silvaco ATLAS Technology Computer Aided Design (TCAD), we simulated and optimized the performance of back-side contact thin-film solar cells. In such a design, both anode and cathode contacts are placed on the same side of a device, resulting in no shadowing of incoming light. The replacement of the AlGaAs emitter with a Schottky junction was simulated and evaluated and compared to the original back-side contact design. Finally, a method of improving the Schottky barrier height of the Schottky design was simulated and evaluated.

THIS PAGE INTENTIONALLY LEFT BLANK

TABLE OF CONTENTS

LIST OF FIGURES

LIST OF TABLES

THIS PAGE INTENTIONALLY LEFT BLANK

LIST OF ACRONYMS AND ABBREVIATIONS

AlGaAs	aluminum gallium arsenide
AM	air mass
As	arsenic
AUGN	Silvaco ATLAS electron auger recombination parameter
AUGP	Silvaco ATLAS hole auger recombination parameter
COPT	Silvaco ATLAS radiative recombination parameter
E_c	conduction band energy level
E_g	bandgap energy level
ELO	epitaxial lift-off
E_v	valance band energy level
FF	fill factor
GaAs	Gallium-Arsenide
Ge	Germanium
k	Boltzmann constant
MOCVD	metal organic chemical vapor deposition
n	electron carrier concentration
n-type	doped semiconductor with a majority carrier of electrons
NPS	Naval Postgraduate School
p	hole-carrier concentration
p-type	doped semiconductor with a majority carrier of holes
PV	Photovoltaics
PT	Platinum
q	charge of an electron
RT	ray tracing
Si	Silicon
SRH	Shockley-Read-Hall
TAUN	Silvaco ATLAS electron lifetime parameter
TAUP	Silvaco ATLAS hole lifetime parameter
TF	Thin Film
Zn	Zinc

THIS PAGE INTENTIONALLY LEFT BLANK

ACKNOWLEDGMENTS

I’d like to thank my extremely bored wife, Megan, for listening to me for countless hours while I explain the superposition of an electron, the probability that we are living in a simulation, and the incredible magnitude of the speed of light. I’d also like to thank my thesis advisors, Sherif Michael and Matthew Porter, for their immeasurable patience and guidance.

THIS PAGE INTENTIONALLY LEFT BLANK

I. INTRODUCTION

Solar cells are a technology which allow for clean, sustainable energy generation using sunlight. As global energy requirements continue to grow, increasing research is needed to make solar energy generation cheap and efficient. Silicon (Si) is currently responsible for 96% of the total photovoltaic (PV) market [1]; however, due to the indirect bandgap of Si, solar cell panels fabricated from Si are traditionally required to be several hundred microns thick for adequate light absorption and are, thus, heavy and inflexible. A large part of ongoing research involves the investigation of new solar cell materials. Advancements in the fabrication of thin-film single-junction solar cells show significant promise due to their increasingly low cost, manufacturability, and high power density [2]. Gallium Arsenide (GaAs) shows particular promise due to the direct bandgap of the material, which allows for GaAs solar cells to be extremely thin. Furthermore, the bandgap of GaAs is nearly ideal for solar cell fabrication as it is small enough to allow for absorption of the majority of the wavelengths of the solar spectrum while having a large enough bandgap for an adequate built-in voltage.

Due to advances in GaAs fabrication techniques, such as epitaxial lift-off (ELO) and metal organic chemical vapor deposition (MOCVD), the fabrication of high quality thin-film GaAs solar cells has recently become possible. Thin-film GaAs cells in just ten years have greatly surpassed the energy efficiency of Silicon (Si) single-junction solar cells, surpassing 28.8% efficiency [3]. Due to up-front costs and complexities with the growth and handling of GaAs solar cells there are only a handful of companies that currently produce GaAs solar cells; however, due to wafer reuse in ELO cell fabrication, manufacturing GaAs solar cells is becoming less prohibitive. Further cost reductions can still be achieved through the use of novel solar cell fabrication methods, which reduce the number of processing steps or materials use.

The objective of this thesis is to investigate the combined performance of several uncommonly used methods of fabricating thin-film GaAs solar cells which show promise in reducing the cost of cell fabrication. Using Silvaco ATLAS technology computer aided design (TCAD), we simulated and optimized the performance of back-side contact thin-

film solar cells. In such a design, both anode and cathode contacts are placed on the same side of a device, resulting in no shadowing of incoming light. The replacement of the AlGaAs emitter with a Schottky junction is then simulated and evaluated in comparison to the original back-side contact design. Finally, a method of improving the Schottky barrier height of the Schottky design is simulated and evaluated.

A. PRIOR WORK

The Naval Postgraduate School (NPS) has used Silvaco ATLAS for over fifteen years to successfully design, model, and optimize solar cells. The first NPS thesis on this topic was published by Michalopoulos, who populated the ATLAS database with the electrical and optical properties of exotic material used in advanced solar cells [4]. Using Silvaco ATLAS, Michalopoulos was able to match the characteristics found in literature of a single junction, dual junction, and triple junction solar cell. Next, Konstantinos designed, modeled, and optimized with Silvaco ATLAS a dual-junction Copper Indium Gallium Selenide (CIGS) thin-film solar cell that achieved 20.3% efficiency [5]. D. Columbus used Silvaco ATLAS to further increase the thin-film CIGS solar cell efficiency by optimizing the thickness layers for various band gaps, achieving an industry record efficiency of 22.4% [6]. In 2015, Green published a thesis on a novel back-surface-contact thin-film silicon-based solar cell modeled with Silvaco ATLAS [7]. Later that year, Katzman published literature on simulating several different methods of creating thin-film CIGS solar cells using Silvaco ATLAS [8]. Lastly, O'Connor published a dissertation which relied on Silvaco ATLAS to design and simulate several novel high-efficiency, back-surface-contact solar cells [9].

B. THESIS ORGANIZATION

This thesis is organized as follows. In Chapter II, we cover the basics on semiconductor physics, solar cell fundamentals, and introduce the modeling software Silvaco ATLAS. In Chapter III, we cover the design, simulation, and optimization of several advanced solar cells. The results and potential future work are discussed in Chapter IV.

II. BACKGROUND

This chapter will serve as an introduction into semiconductors, formation of the potential barrier, the current transport process, the underlying the physics and behavior of solar cells, and the Silvaco ATLAS simulation tool.

A. SEMICONDUCTOR BASICS

A semiconductor is a material with resistivity between that of a conductor (low resistivity) and an insulator (high resistivity). A semiconductor is traditionally composed of elements that contain four electrons in its outermost, or valence, band. As each atom desires to have eight electrons in its outermost shell, the semiconductor element covalently bonds with a neighbor atom. Single-element semiconductors are chosen from column IV of the periodic table, such as Si or Germanium (Ge), which each have four electrons in their valence shell. Multiple element semiconductors, such as GaAs, are made from bonding Group III-to-V or II-to-VI elements to also achieve eight electrons in the valence shell of the molecule [9].

1. Electronic Band Structure

The bandgap of a semiconductor is the region between the valence and conduction band [9]. The valence band E_v contains the outermost electrons at the lowest energy level. If an electron gains sufficient energy, it transitions, or jumps, to a higher available energy state in the conduction band E_c. This forms an electron-hole pair where the electron now occupies the conduction band, and a positive charge (hole) is left behind in the valence band. The bandgap E_g, depicted in Figure 1, contains no energy levels for an electron to occupy.

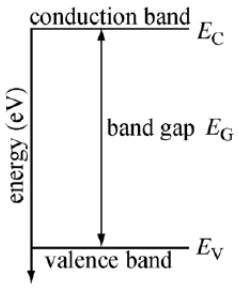

Figure 1. Bands of a Molecule. Source: [9].

a. Intrinsic Semiconductor

An intrinsic semiconductor describes a perfect lattice structure where each atom has eight valence electrons in its outermost shell [10]. In intrinsic material the concentration of electrons and holes are equal and can be found with

$$n_i = n = p = \sqrt{N_C N_V \exp(-E_g / kT)} \tag{1}$$

where n_i is the intrinsic carrier concentration, n is the number of electrons, p is the number of holes, N_C is the density of states in the conduction band, N_V is the density of states in the valence band, k is the Boltzmann's constant, and T is temperature. When the temperature is at 300 K N_C and N_V are denoted $N_{C,300}$ and $N_{V,300}$ are readily available numbers for semiconductor materials.

At very low temperatures all energy states in the conduction band are occupied and all other energy states are empty [9]. The highest energy level occupied is named the Fermi level E_F [11]. As temperature increases, some electrons absorb sufficient thermal energy to transition to higher energy states greater than the Fermi level. The Fermi-Dirac function describes the mobility of electrons at thermal equilibrium and is given by [11]

$$F(E) = \frac{1}{1 + \exp(\frac{E_I - E_F}{kT})} \tag{2}$$

where E_I is the middle of the bandgap in an intrinsic semiconductor.

b. Extrinsic Semiconductor

Intentional impurities, known as dopants, are added to an intrinsic semiconductor to form extrinsic semiconductors through a process known as *doping*. As seen in Figure 2, when a Group III or V element is introduced to a pure Ge molecule there is an extra electron or hole, respectively, in the valence shell.

In *n*-doped material there are more electrons than holes. The extra electrons from the doping process require a small amount of energy to ionize and leave a hole. In *p*-doped material there are more holes than electrons.

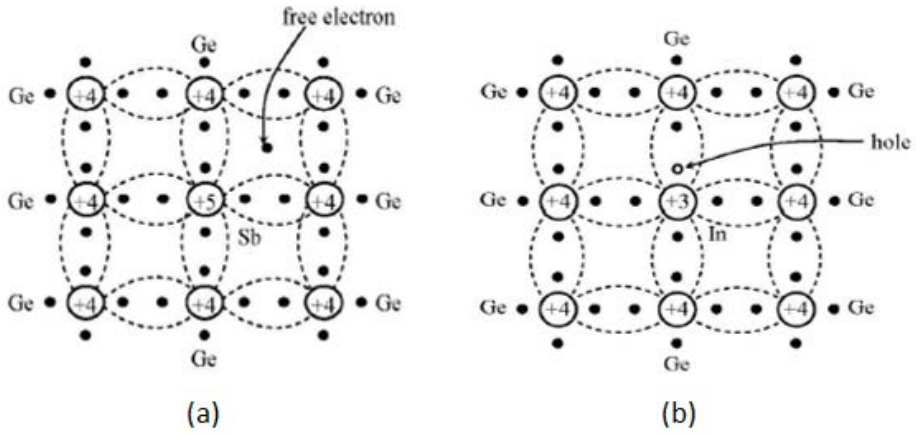

Figure 2. (a) Ge Molecule Doped with Antimony (Sb) Forming a *n*-type Semiconductor and (b) Ge Molecule Doped with Indium (In) Forming a *p*-type Semiconductor. Adapted from [12].

Due to the introduced donors and acceptors, the Fermi level is no longer located in the middle of the bandgap. As seen in Figure 3, a *n*-doped semiconductor has a Fermi level that is closer to the conduction band. This is because the probability of finding an electron near the conduction band is greater since there are more loosely bound electrons. Similarly, a *p*-doped semiconductor has a Fermi level that is closer to the valence band as the probability of finding an electron near the conduction band is smaller.

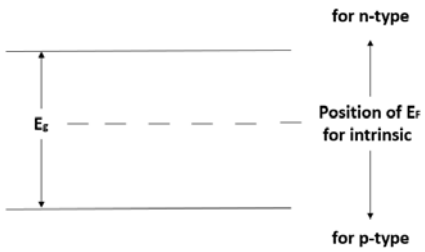

Figure 3. Fermi Level Shift Due to Doping. Source: [11].

The electron and hole concentrations in an extrinsic semiconductor are found by

$$n = N_C \exp\left(\frac{E_F - E_C}{kT}\right) \tag{3}$$

and

$$p = N_V \exp\left(\frac{E_V - E_F}{kT}\right) \tag{4}$$

where $N_{C,300}$ and $N_{V,300}$ values are used. Due to doping, E_F is no longer equal to E_I and is computed from

$$E_F = \frac{E_C + E_V}{2} + \frac{kT}{2}\ln\left(\frac{N_V}{N_C}\right) + \frac{kT}{2}\ln\left(\frac{n}{p}\right). \tag{5}$$

When highly doped, the Fermi level may pass the conduction or valence band edge and is known as *degenerate*; otherwise, for low doping the semiconductor is said to be *nondegenerate* [11].

2. *p-n* Junction Diode

A *p-n* junction diode is formed when one side of a semiconductor differs from the other side, say from doping or differing elements. Most commonly one side of the semiconductor is *p*-doped while the other is *n*-doped. The electrons located in the high, negatively concentrated *n*-doped side *diffuse* to the lower, negatively concentrated *p*-doped side; similarly, holes located in the high, positively concentrated *p*-doped side *diffuse* to the lower, positively concentrated *n*-doped side. This diffusion of majority charge carriers causes a potential difference, and an electric field forms with charge increasing from *n*-

doped to *p*-doped side. Due to the electric field, the minority carriers in the *n*-doped side *drift* to the *p*-doped side, and minority charge carriers in the *p*-doped side *drift* to the *n*-doped side. This exchange of electrons and holes continues until thermal equilibrium is reached. Depicted in Figure 4 is a *p*-*n* junction once thermal equilibrium is reached and the depletion region has formed.

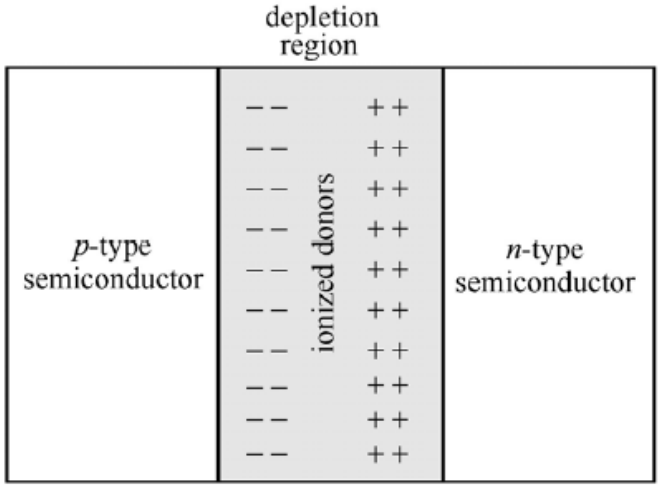

Figure 4. Basic *p*-*n* Junction with Depletion Region. Source: [9].

The presence of the electric field causes a built-in voltage V_{bi} representing the energy necessary for a majority charge carrier to pass through the internal electric field. At un-biased equilibrium with no illumination, the Fermi level remains flat; thus, the conduction and valence bands bend in the depletion region [13]. This phenomenon is shown in Figure 5.

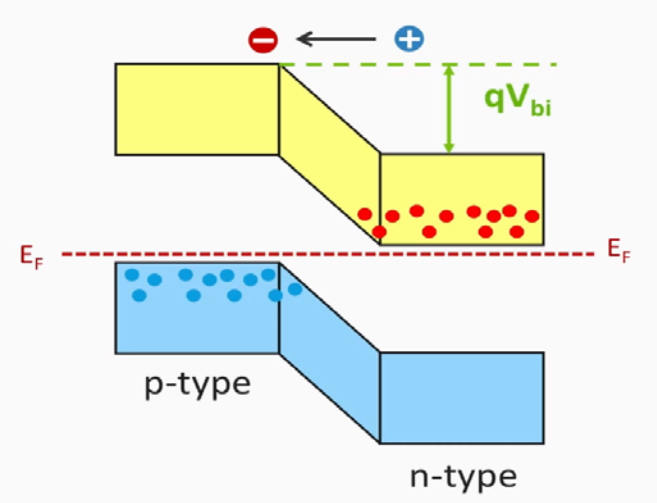

Figure 5. Conduction and Valence Band Bending in the Depletion Region Due to Internal Electric Field. Source: [13].

The built-in voltage V_{bi} is computed with

$$V_{bi} = \frac{kT}{q} \ln\left(\frac{N_D^+ N_A^-}{n_i^2}\right). \tag{6}$$

The width of the depletion region on the *n*-type and *p*-type sides are calculated as

$$X_n = W \frac{N_A^-}{N_A^- + N_D^+} \tag{7}$$

and

$$X_p = W \frac{N_D^-}{N_A^- + N_D^+} \tag{8}$$

where W is the total width of the depletion region and can be computed with

$$W = X_n + X_p = \sqrt{\frac{\varepsilon_r \varepsilon_0}{q}\left(\frac{N_A^- + N_D^+}{N_A^- N_D^+}\right) V_{bi}} \tag{9}$$

where ε_r is the relative permittivity and ε_0 is the free-space permittivity.

3. Schottky Junction

A Schottky junction is formed between a semiconductor and a metal contact due to their differing work functions. The work function is the minimum amount of energy required to free an electron from the outermost conduction band to the vacuum level [10]. Electron affinity is commonly used in reference to a semiconductor and is the energy required to free an electron from the Fermi to vacuum level. The barrier height θ_{Bn0} is the difference between the metal work function, and the electron affinity of a semiconductor and is found from

$$\theta_{Bn0} = \phi_m - \chi \tag{10}$$

where ϕ_m is the work function of the metal and χ is the electron affinity of the semiconductor. Shown in Figure 6, as the gap between a metal and semiconductor is reduced, the electrons in the semiconductor with a higher energy state diffuse to the metal as they seek equilibrium. As the two media come into contact and equilibrium is sought, the Fermi level on both sides lines up. This in turn lowers the Fermi level of the semiconductor by an amount equal to the work function of the metal [10]. Similar to a *p*-*n* junction, due to the diffusion of majority charge carriers from the semiconductor to the metal a depletion layer forms with a width found from

$$W = \sqrt{\frac{2\varepsilon_s}{qN_D}\left(V_{bi} - V_a - \frac{kT}{q}\right)} \tag{11}$$

where ε_s is the semiconductor permittivity.

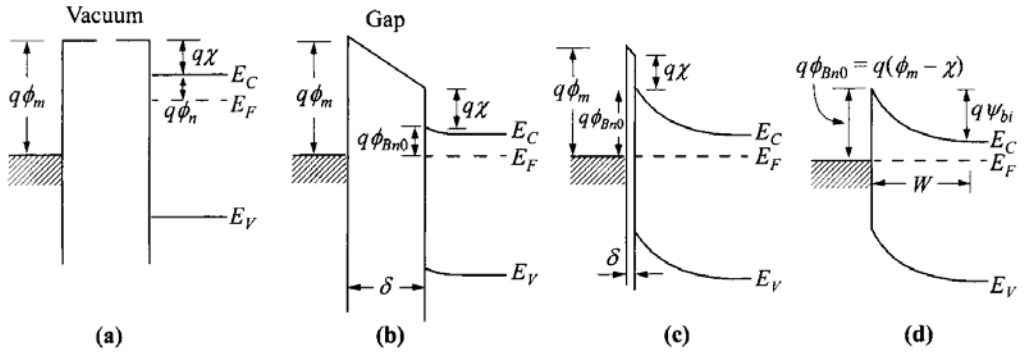

Figure 6. Transition of the Energy-Band Diagrams from (a) to (d) of a Metal Semiconductor Contact as the Gap δ Is Removed. Source: [10].

4. Carrier Transport

Drift current densities J_p^{drift} and J_n^{drift} for holes and electrons, respectively, are caused by the presence of an electric field within the semiconductor [14]. Minority charge carriers *drift* in the direction of the electric field. The net effect is that electrons and holes move at a constant velocity named drift velocity v_d found from

$$|v_d| = \left|\mu \vec{E}\right| \tag{12}$$

where μ is the carrier mobility and $\vec{E}$ is the applied electric field. The drift current densities can be found from

$$J_p^{drift} = q\mu_p p \vec{E} \tag{13}$$

and

$$J_n^{drift} = q\mu_n n \vec{E} \tag{14}$$

where q is the charge of an electron, μ_p and μ_n are mobilities, and n or p are electron or hole concentrations, respectively.

Diffusion current densities J_p^{diff} and J_n^{diff} are caused by the high concentration of electrons or holes and are given by

$$J_p^{diff} = -qD_p \nabla p \tag{15}$$

and

$$J_n^{diff} = qD_n \nabla n \tag{16}$$

where D is the charge diffusion coefficients given by

$$D = \frac{kT\mu}{q} \tag{17}$$

and ∇ is the gradient of the carrier densities [15]. The average distance an electron travels before recombination is referred to as diffusion length and can be computed as

$$L = \sqrt{D\tau} \tag{18}$$

where τ is the average time the free electron exists [9].

The total current density is the sum of the drift and diffusion components found from

$$J_p = J_p^{drift} + J_p^{diff} = q\mu_p p\vec{E} - qD_p \nabla p \tag{19}$$

and

$$J_n = J_n^{drift} + J_n^{diff} = q\mu_n n\vec{E} + qD_n \nabla n\,. \tag{20}$$

5. Carrier Recombination

When a photon generates an electron-hole pair, it does not always contribute to the electric current as there are losses due to recombination. The losses due to recombination are grouped into two classes, *direct* and *indirect* recombination. Direct recombination, or band-to-band recombination, is when an electron and hole recombine directly between the valence and conduction band [9]. Indirect recombination is due to an outside force or lattice defect.

Two forms of direct recombination are radiative and auger. Radiative recombination R_{rad} is when an electron and hole recombine directly between the valence and conduction bands, and the energy is released as a photon. Auger recombination R_{auger} is similar except the energy is released as vibration through the lattice structure [9].

A form of indirect recombination is trap-state recombination R_{trap}. Trap recombination, also known as Shockley-Read-Hall (SRH) recombination, is due to trap states that "trap" free electrons. These traps are commonly found at the surface, near heterojunctions, at etching locations, and where differing doping concentration interface [14]. The total recombination rate can be easily found from $R_T = R_{trap} + R_{auger} + R_{rad}$.

6. Governing Semiconductor Equations

Poisson's and semiconductor continuity equations in large fully describe the operation of most semiconductors [16]. The equations describe the local conservation of electron and hole concentration, accounting for carrier generation and recombination [14]. Poisson's equation can be generalized to

$$\frac{\partial(\varepsilon \vec{E})}{\partial x} = q(p - n + N_D^+ - N_A^-) \tag{21}$$

where ε is the relative permittivity and N_D^+ or N_A^- are the donor and acceptor concentrations, respectively. The semiconductor continuity equations are

$$\frac{\partial p}{\partial t} = \frac{1}{q}\frac{\partial J_p}{\partial x} + G_p - R_p \tag{22}$$

and

$$\frac{\partial n}{\partial t} = \frac{1}{q}\frac{\partial J_n}{\partial x} + G_n - R_n \tag{23}$$

where G represents the carrier generation rates in $cm^{-3}s^{-1}$ and R represents the carrier recombination rates in $cm^{-3}s^{-1}$.

B. SOLAR CELLS

Arguably, the most important physical characteristic of a solar cell is the materials band gap [10]. The bandgap not only determines how much of the solar spectrum is capable of generating current but also determines the magnitude of the built-in voltage. The equation that describes the relationship between the wavelengths of light and energy is given by

$$h\nu(eV) = h\frac{c}{\lambda} = \frac{1.24}{\lambda(\mu m)} \tag{24}$$

where h is Plank's constant, ν is frequency, c is the speed of light, and λ is wavelength. As shown in Figure 7, semiconductors with a band gap less than 1.7 eV absorb most of the solar spectrum, with the peak absorption occurring at roughly 1.4 eV [15].

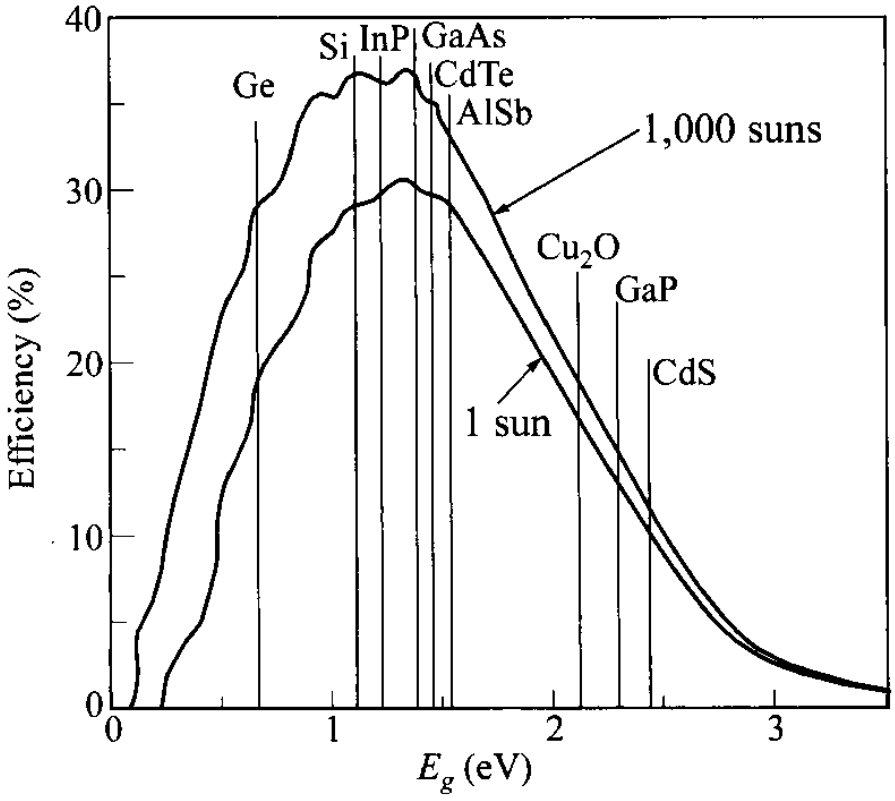

Figure 7. Ideal Material Band-Gap for Solar-Cell Efficiency. Source: [10].

A *direct* bandgap semiconductor refers to when the conduction band and valence band line-up at the same crystal momentum. An *indirect* bandgap semiconductor occurs when the two bands do not align. In the direct bandgap case, a single photon can ionize an electron. For an indirect bandgap semiconductor, ionizing an electron is more complicated.

In the *indirect* bandgap semiconductors case, a collision with a photon and electron excite the electron, but since the conduction and valence bands do not align, a second step is required to match the momentum of the electron and conduction band. Low-energy particles with high momentum, known as phonons, typically facilitate the required second step [14] As depicted in Figure 8, photon absorption frees an electron from the valence band, and phonon absorption moves the electron to match the crystal momentum of the conduction band.

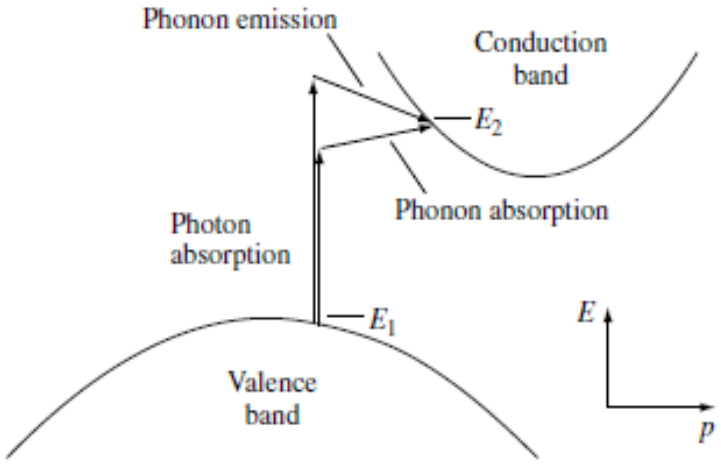

Figure 8. Electron Ionization for an Indirect Bandgap Semiconductor. Source: [14].

1. Solar Irradiation

Approximately 70 percent of the solar radiation successfully travels through the atmosphere of the Earth [15]. Air mass zero (AM0) refers to the solar irradiation in space, AM1 refers to the solar irradiation at sea level, and AM1.5 represents terrestrial irradiation [9]. The difference between AM0 and AM1.5 is seen in Figure 9. In this thesis, we focus on AM1.5.

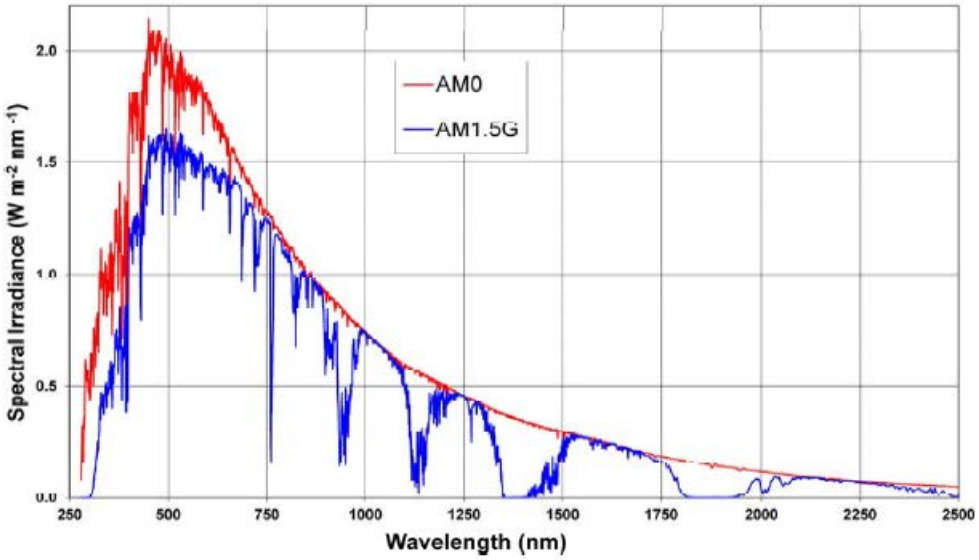

Figure 9. Solar Irradiation Spectrum at AM0 and AM1.5. Source: [9].

If a photon has energy greater than the bandgap of the solar cell material, the photon is capable of being absorbed and transitioning an electron from valence to conduction band, creating an electron-hole pair. Each photon is capable of generating only a single electron-hole pair, and any excess energy is lost as heat within the device [15].

The absorption coefficient α is the inverse of the average photon penetration depth, or the inverse of the distance a photon travels [15]. A large absorption coefficient indicates that the photon is absorbed near the surface (low penetration depth). The rate at which an electron-hole pair is generated is known as the carrier-generation rate G and can be computed with

$$G = \alpha F(0)\exp(-\alpha x) \tag{25}$$

where the absorption coefficient α is essentially zero for $h\nu < E_g$ and larger than 10^4 cm^{-1} for $h\nu \geq E_g$, x is the average distance a photon travels before absorption, and $F(0)$ is the photon flux with $x = 0$.

As shown in Figure 10, a photon with an incident angle θ_i that encounters the interface between two different media reflects the wave at reflected angle θ_r and refracts the wave at transmitted angle θ_t [17]. These values can be found with

$$\theta_i = \theta_r \tag{26}$$

and

$$\frac{\sin(\theta_i)}{\sin(\theta_t)} = \frac{n_2}{n_1} \tag{27}$$

where n_1 and n_2 are the refractive indices of each media [18].

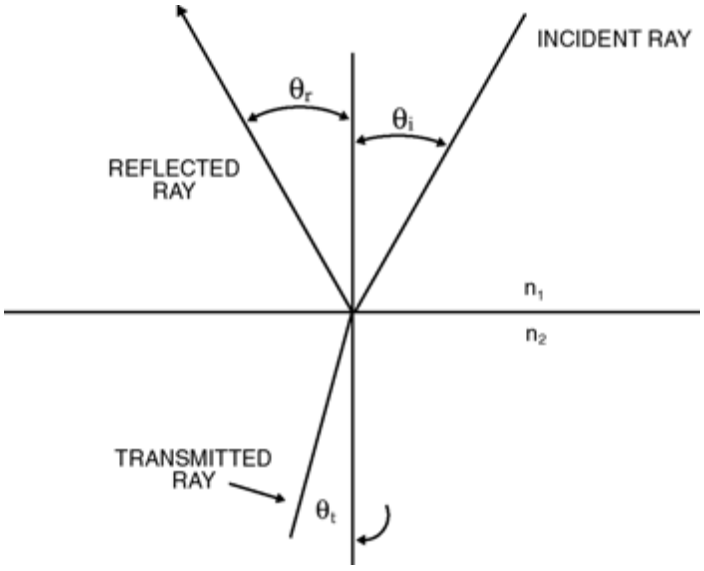

Figure 10. Angles of Incidence, Reflection, and Transmission. Source: [18].

2. Solar Cell Operation

A succinct demonstration of the interaction between a semiconductor with a formed depletion region and high-energy photons is shown in Figure 12. The yellow lines represent photons from the sun which have energy greater than the semiconductors bandgap. Each photon has the opportunity to collide and form an electron-hole pair. When a photon generates an electron-hole pair in the *p*-type region, the freed electron diffuses to the *n*-type region due to the electric field, while the freed hole is repulsed by the electric field. In the *n*-type region, a freed electron diffuses to the *p*-type region due to the electric field, while a freed electron is repulsed by the electric field. If an external load is connected, electrons flow and current is generated.

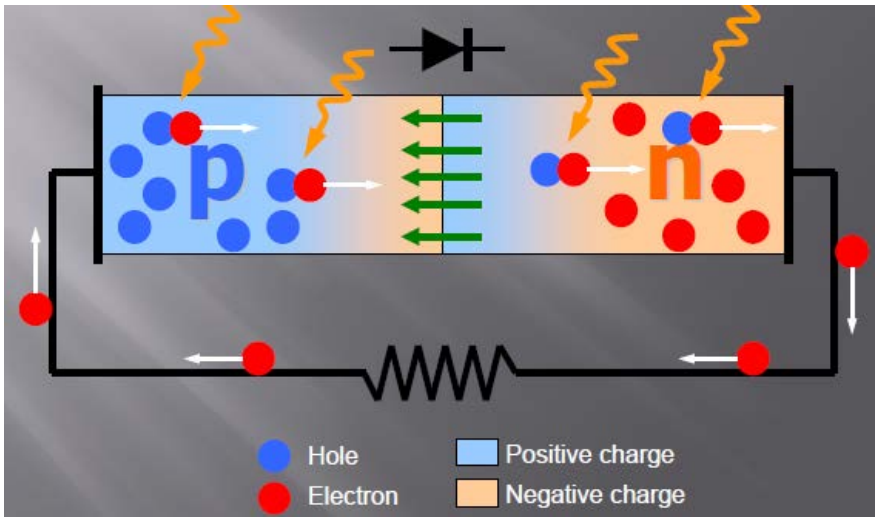

Figure 11. Operation of a Solar Cell. Source: [12].

3. Solar Cell Parameters

Some parameters that are specific to describing solar cells, shown in Figure 11, are short circuit current density J_{SC}, open circuit voltage V_{OC}, maximum current I_{MP}, maximum voltage V_{MP}, maximum power point MPP, fill factor FF, and efficiency μ [16]. Short circuit current I_{SC} is the maximum current through a *p*-*n* junction, and J_{SC} is the I_{SC} per unit area in mA/cm^2 [14]. The V_{OC} is the maximum voltage possible across a

p-n junction. The current-voltage (I-V) characteristic of a typical solar cell is not linear; therefore, MPP occurs when the current and voltage product is at the maximum value. The FF is the difference between the MPP and the product of V_{OC} and I_{SC}.

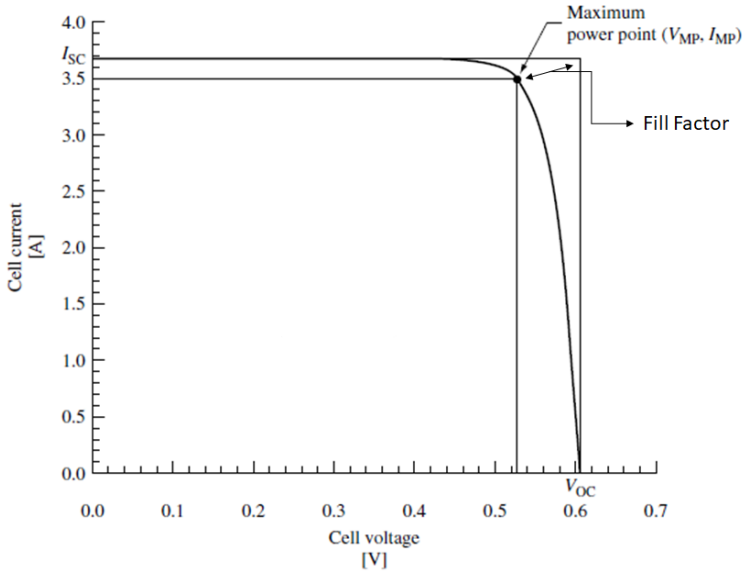

Figure 12. Illustration of Several Key Solar Cell Parameters. Adapted from [14].

The fill factor is calculated from

$$FF = \frac{MPP}{V_{OC} I_{SC}} = \frac{V_{MP} I_{MP}}{V_{OC} I_{SC}} \tag{28}$$

where V_{MP} and I_{MP} are the points at which MPP occur. The solar cell efficiency can be found with

$$\mu = \frac{MPP}{P_{in}} \tag{29}$$

where P_{in} is the power from the sun (input power) [14].

C. SILVACO ATLAS

TCAD is useful to design, test, and optimize solar cell ideas prior to actual device fabrication. Silvaco ATLAS is a semiconductor simulator that has been used by industry and universities for over 20 years [18]. Silvaco ATLAS has a built-in database for common semiconductor material properties. The characteristics for exotic materials that are commonly used in advanced semiconductors can be manually inputted. When designing a solar cell, Silvaco ATLAS allows for easily modifiable dimensions and doping concentration of each region. Underlying each region, the user defines a grid-based mesh. The mesh must be dense in the regions with rapidly varying carrier energy such as the depletion region, heterojunctions, electrodes, interfaces between different doping concentration, and regions with differing refractive indices.

SILVACO Atlas uses Luminous to model light propagation and absorption within a solar cell. One available Luminous physical model is Ray Tracing (RT) where light is treated as a point particle [18]. RT is useful as it is not computationally expensive and hundreds of simulations can be done relatively quickly. The Luminous RT model uses an incident beam that is split into a series of rays that sum to cover the width of simulated device [18]. Each incident beam is split at the interface between mediums into a reflected and transmitted rays. The reflection and transmission coefficients, *RE* and *TR* respectively, are defined within the ATLAS User's Manual as

$$E_r = \frac{n_2 \cos(\theta_i) - n_1 \cos(\theta_t)}{n_2 \cos(\theta_i) + n_1 \cos(\theta_t)} E_i , \tag{30}$$

$$E_t = \frac{2n_1 \cos(\theta_i)}{n_1 \cos(\theta_t) + n_2 \cos(\theta_i)} E_i , \tag{31}$$

$$RE = \left(\frac{E_r}{E_i} \right)^2 , \tag{32}$$

and

$$TR = \left(\frac{E_t}{E_i} \right)^2 \frac{n_2}{n_1} \frac{\cos(\theta_t)}{\cos(\theta_i)} \tag{33}$$

where E_i is electric field of the incident wave, E_r is the field of the reflected wave, and E_t is the field of the transmitted wave. Silvaco ATLAS uses the REFLECTS parameter to specify the number of rays to be traced. This parameter can lead to very long simulation times and is advised to be used wisely [18]. For this thesis the REFLECTS parameter was set to one, meaning ten rays are traced for each single ray of incidence on a three material layer device.

Based on the illumination profile, Silvaco ATLAS uses Newton's method to iteratively solve for the roots of the governing semiconductor non-linear differential equations at each grid point [18]. Silvaco ATLAS also solves for several other parameters, namely SRH recombination rate, auger recombination rate, radiative recombination rate, Fermi-Dirac statistic, electron and hole mobility based on doping concentration, and ohmic and Schottky contact interactions.

III. DESIGN EXPLORATION

The dominant material used in photovoltaic devices today is silicon [1]. Due to silicon being an *indirect* bandgap material, it is necessary for silicon PV devices to be several hundred microns thick or to employ advanced light trapping techniques [14]. Light trapping is a method to "trap" the light within the device; however, the techniques are costly, difficult to achieve, and add additional defect states which increase SRH recombination [19].

Other materials theoretical efficiencies are higher than silicon, but due to their cost, limited resource, or difficulty in handling have not yet overthrown the clinch silicon has on market. GaAs is a very promising material for photovoltaics due to its ideal bandgap. Also, GaAs is a *direct* bandgap material and an ideal candidate for thin-film. Alta-Devices thin-film GaAs cell currently holds the record for the most efficient single-junction solar cell at 28.5% efficiency.

A. BASELINE SOLAR CELL

The solar cell chosen, shown in Figure 13, as an initial baseline is based on Alta-Devices commercially available 26% efficiency cell. The code used to simulate and test the cell depicted in Figure 14 is shown in Appendix A. The cathode at the top of the cell shadows, or blocks, 7% of the sun's light, which is a common amount for a solar cell with contacts on the front. Realistic GaAs material properties were chosen based on findings in literature. Wang *et al.* found GaAs auger recombination properties, denoted AUGN and AUGP in Silvaco ATLAS, to be 7×10^{-30} cm^6s^{-1} [20]. Wang *et al.* also found GaAs electron and hole lifetime parameters, denoted TAUN and TAUP in Silvaco ATLAS, to be 5.10×10^{-7} s. Hooft *et al.* found GaAs radiative recombination rates, COPT, to be 1.3×10^{-10} cm^3s^{-1} [21]. The dimensions and doping concentrations for the cell are shown in Table 1.

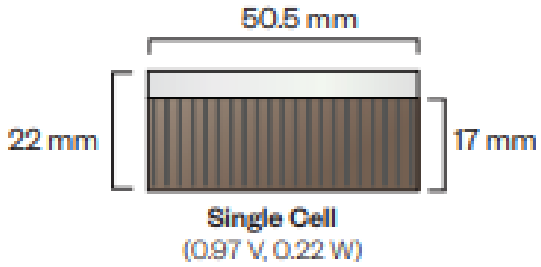

Figure 13. Alta Devices Record Efficiency Cell. Source: [22].

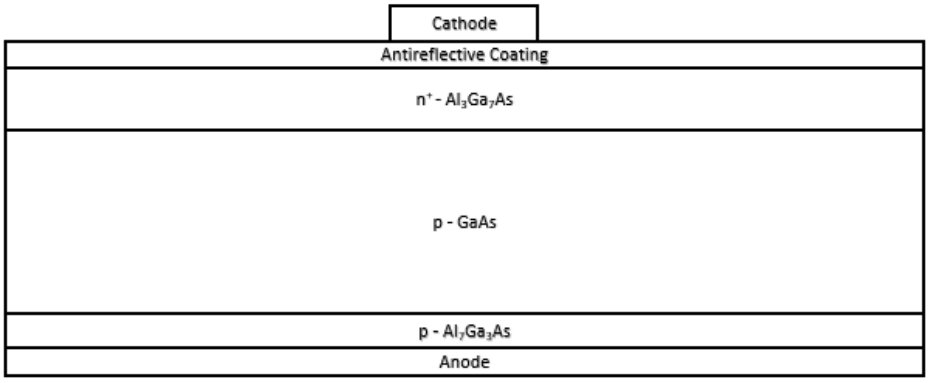

Figure 14. GaAs Baseline Solar Cell

Table 1. Dimensions and Doping Parameters of GaAs Baseline Solar Cell

Parameter	Value
n^+-type Al_3Ga_7As Thickness	0.01 µm
n^+-type Al_3Ga_7As Doping	1×10^{20} cm^{-3}
p-type GaAs Thickness	3.0 µm
p-type GaAs Doping	1×10^{16} cm^{-3}
p-type Al_7Ga_3As Thickness	0.3 µm
p-type Al_7Ga_3As Doping	1×10^{16} cm^{-3}

Using the MATLAB code in Appendix B, we plotted the I-V characteristic for the baseline solar cell in Figure 15. The cell demonstrated an efficiency of 24.97% with a fill factor of 93.6.

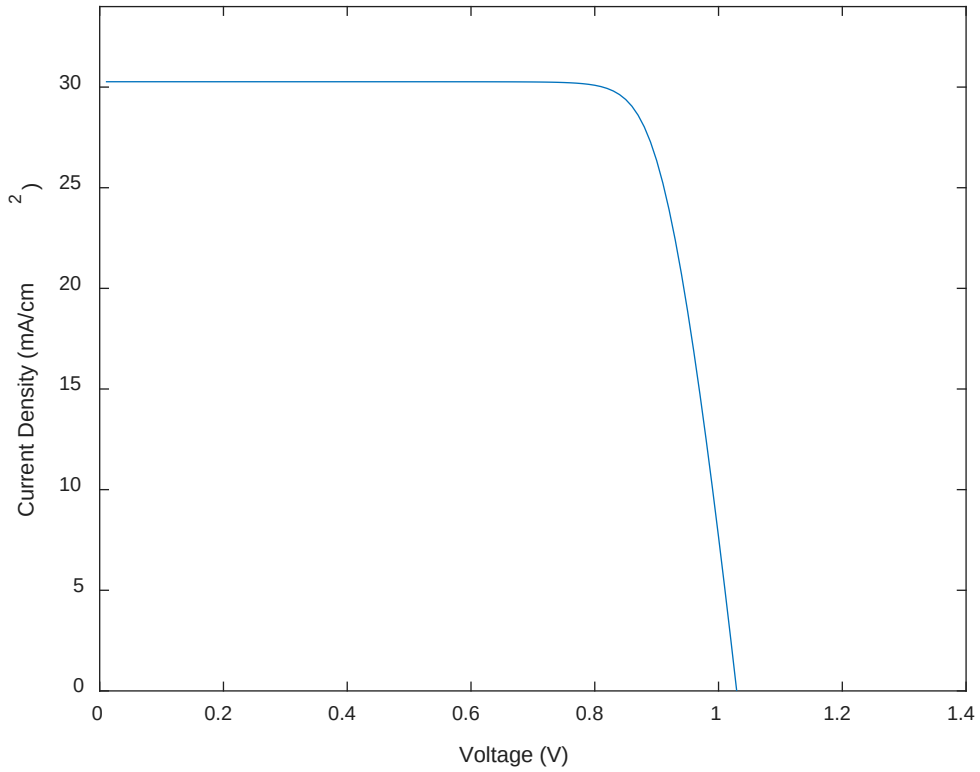

Figure 15. I-V Characteristics for GaAs Baseline Solar Cell

The modeled cell has an efficiency 1% lower than expected. This is most likely due to Silvaco ATLAS not accounting for photon recycling. Photon recycling is when radiative recombination occurs and the emitted photon is reabsorbed within the semiconductor.

Currently, no semiconductor modeling software has a built-in method to account for photon recycling. Letay *et al.* identified a work-around method to incorporate photon recycling in the modelling software *PVObjects* [23]. Similarly, Walker *et al.* identified an iterative process to account for photon recycling with the modeling software *Sentaurus* [24]. Notably, these papers indicate that an increase of one percent efficiency is expected on a solar cell with contacts on the front due to photon recycling; therefore, with photon recycling accounted for, our modeled solar cell is performing as expected.

B. ALL BACK CONTACT SOLAR CELL

Arranging all contacts to the back of the solar cell, henceforth named all-back-contacts (ABC), may yield a higher efficiency since the device will have no shadowing. Shown in Figure 16 is the ABC solar cell based off of Alta Devices patent US8895845B2 which was modeled with Silvaco ATLAS [25].

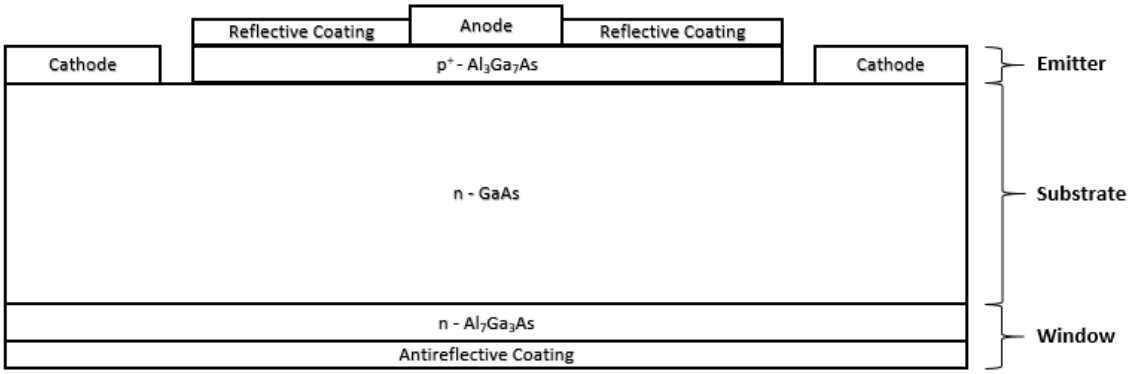

Figure 16. Alta Devices GaAs ABC Solar Cell

The baseline values for the solar cell parameters were obtained from Alta Devices patent. The parameters can be found in Table 2, where the window layer refers to *n*-type Al_7Ga_3As, the substrate layer refers to *n*-type GaAs, and the emitter layer refers to p^+-type Al_3Ga_7As. The range of values for each parameter were chosen based of the patents literature [25].

Table 2. Baseline and Range of Values for Each Parameter

Parameter	Baseline value	Range of Values
Window Thickness	0.02 µm	0.005–0.03 µm
Window Doping	1×10^{16} cm^{-3}	1×10^{16}–1×10^{19} cm^{-3}
Substrate Thickness	3.0 µm	0.5–3.5 µm
Substrate Doping	1×10^{17} cm^{-3}	1×10^{16}–1×10^{19} cm^{-3}
Emitter Thickness	0.3 µm	0.1-2 µm
Emitter Doping	1×10^{19} cm^{-3}	1×10^{17}–1×10^{20} cm^{-3}

1. Device Optimization

Substrate thickness and doping were optimized first while the window and emitter parameters were held at their baseline values. The MATLAB code in Appendix C was used to call Silvaco ATLAS and run a total of four hundred simulations testing twenty substrate thicknesses between 0.5 and 3.5 μm with the combination of twenty substrate doping values between 1×10^{16} and 1×10^{19} cm^{-3}. The Silvaco ATLAS code is given in Appendix D. The results can be seen in Figure 17, which led to an optimal substrate thickness of 2.0789 μm and doping of 1×10^{16} cm^{-3}. The MATLAB code in Appendix E was used to find the peak efficiency of 20.96% with a fill factor of 96.17%.

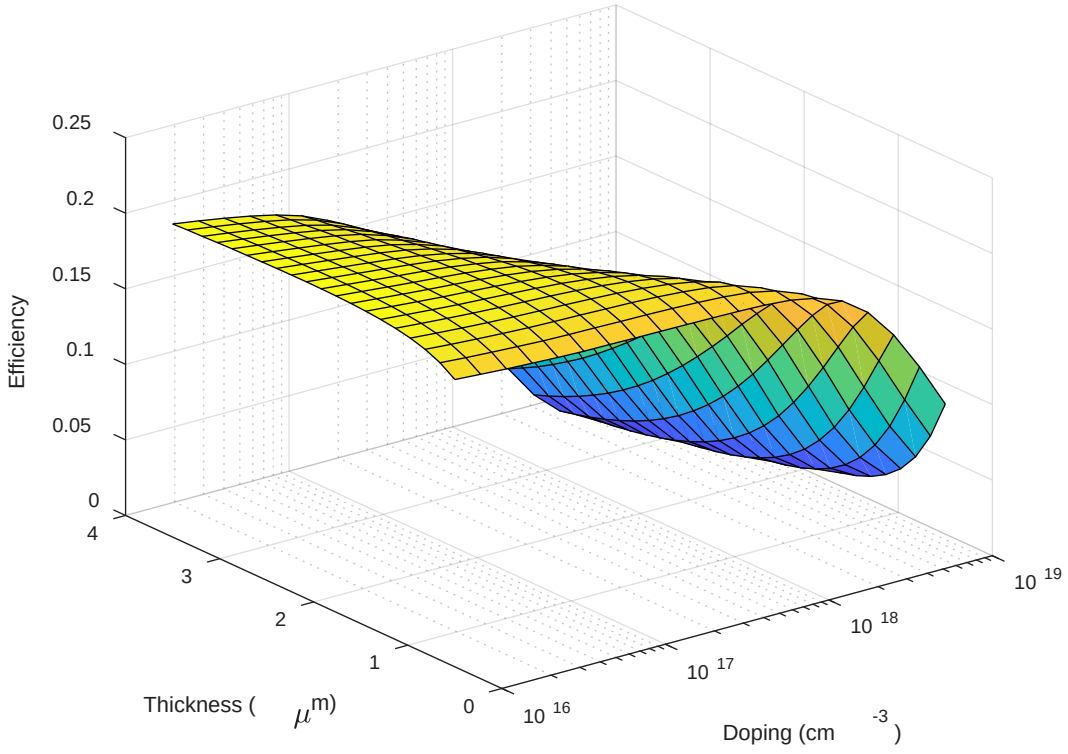

Figure 17. Substrate Thickness and Doping Optimization

The baseline values for the substrate thickness and doping were augmented to the optimized values within Silvaco ATLAS. Using the slightly altered MATLAB code in Appendix C, another set of 400 simulations were run testing twenty emitter thicknesses between 0.1 and 2.0 µm with the combination of twenty substrate doping values between 1×10^{17} and 1×10^{20} cm^{-3}. The results can be seen in Figure 18, which led to an optimal Emitter thickness of 0.03 µm and doping of 8.8587×10^{16} cm^{-3}. The slightly altered MATLAB code in Appendix E was used to find the peak efficiency of 21.00% with a fill factor of 92.91%.

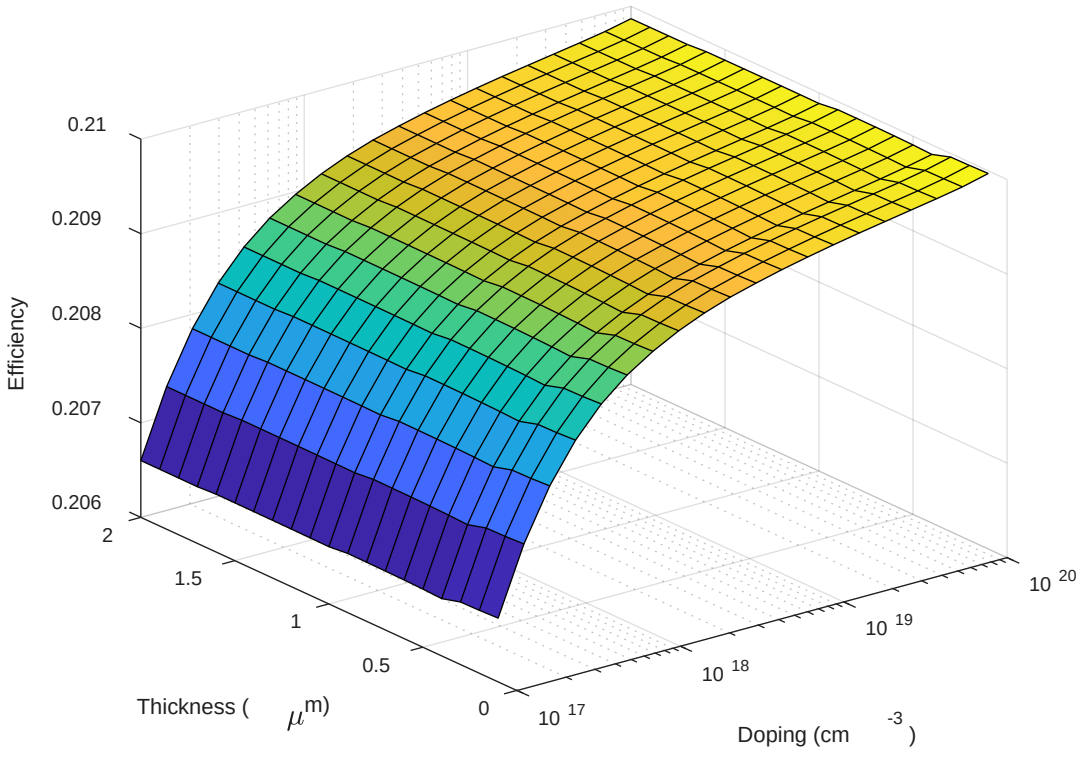

Figure 18. Emitter Thickness and Doping Optimization

The newfound optimum values for the emitter thickness and doping values were updated in the simulation model. Using the slightly altered MATLAB code in Appendix C, another set of 400 simulations were run testing twenty window thicknesses between 0.005 and 0.03 µm with the combination of twenty window doping values between 1×10^{16} and 1×10^{19} cm^{-3}. The results can be seen in Figure 19, which led to an optimal window

thickness of 0.1 μm and doping of 1×10^{20} cm^{-3}. The slightly altered MATLAB code in Appendix E was used to find the peak efficiency of 21.01% with a fill factor of 92.91%.

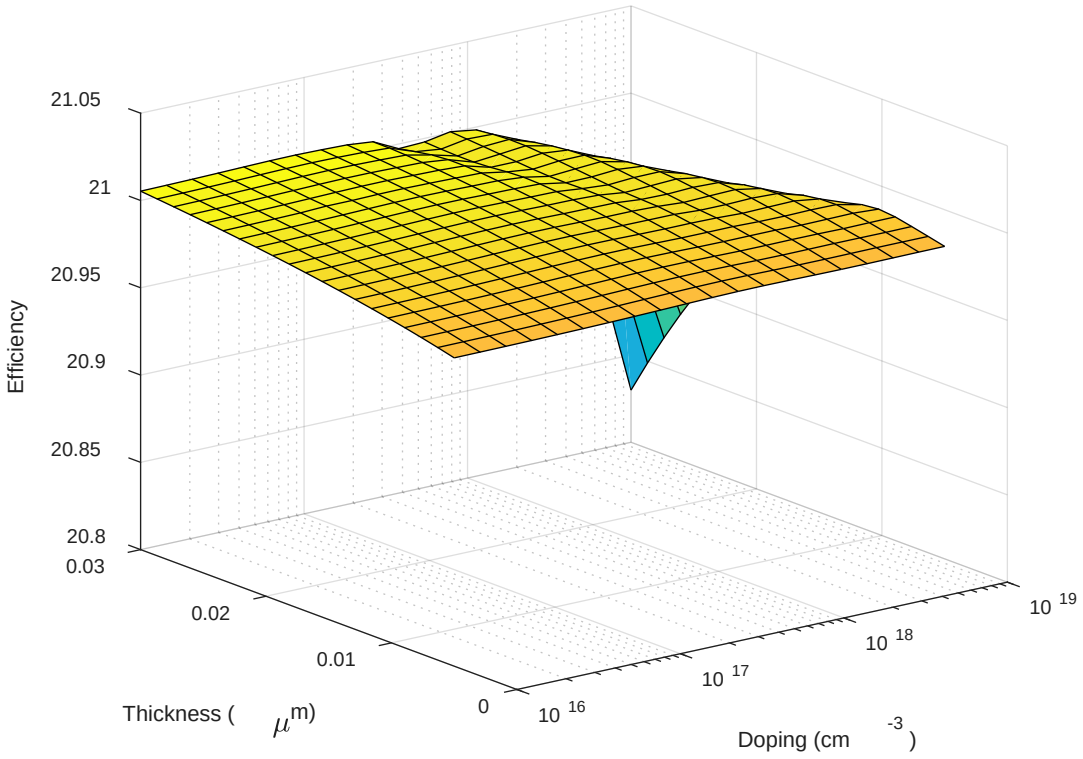

Figure 19. Window Thickness and Doping Optimization

2. Results

The optimized ABC solar cell demonstrated an efficiency that is 4% lower than the front contact solar cell; however, photon recycling most likely has a greater impact on an ABC solar cell due to the nature of photon absorption. A high energy photon is most likely absorbed near the surface of a solar cell. With the baseline design, the *p-n* junction is near the top of cell, and a free electron caused by the absorption of a photon will likely reach the nearby cathode prior to recombination. With the ABC solar cell, a free electron caused by the absorption of a photon near the top of the cell has to travel the thickness of the solar cell and reach the contacts located at the bottom of the cell in order to contribute to the current. A comparison between the total recombination rate of the baseline and ABC solar

cell is shown in Figure 20. Due to the greater amount of recombination in the ABC solar cell, there is a greater increase in efficiency due to photon recycling.

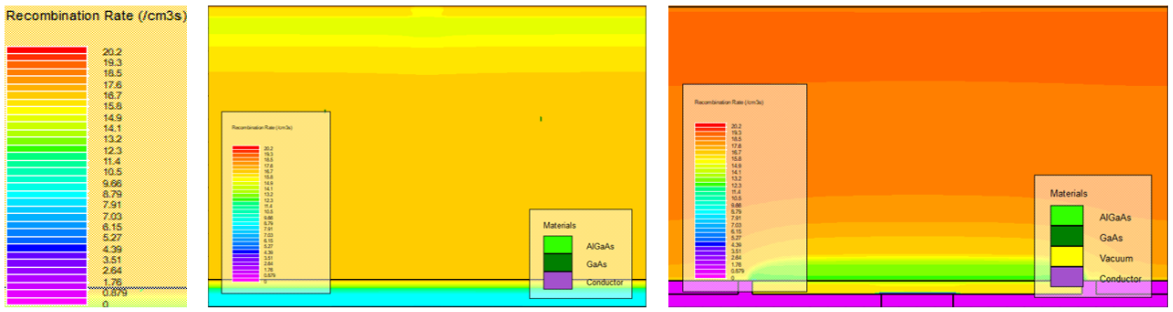

Figure 20. (a) Enlarged Scale of Recombination Rate, (b) Recombination Rate of Baseline Front Surface Cell, and (c) Recombination Rate of an ABC Cell

C. SCHOTTKY SOLAR CELL

With photon recycling accounted for, the ABC solar cell may achieve comparable efficiency to the baseline cell. In this section the *p-n* junction formed from the highly p^+-doped emitter layer is replaced with a Schottky junction. Byrnes *et al.* research showed that a Schottky junction silicon solar cell was able to achieve comparable efficiency to a *p-n* junction cell [26]. Byrnes goes on to state that the elimination of the emitter layer reduces the energy necessary to manufacture the Si PV cell by 35% and reduces SRH and Auger recombination due to less crystal defects. Shown in Figure 21 is the Schottky ABC solar cell design that was modeled with Silvaco ATLAS.

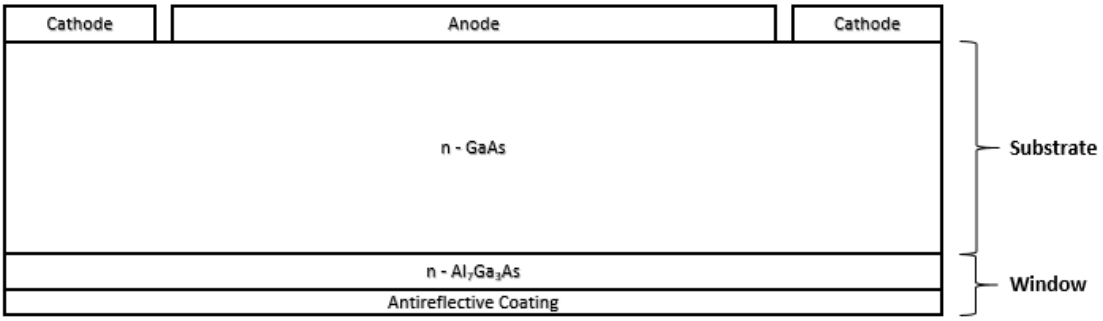

Figure 21. Schottky ABC Solar Cell

The parameters used for the Schottky ABC solar cell, shown in Table 3, are the optimized values found in the previous section. The window layer refers to *n*-type Al_7Ga_3As, and the substrate layer refers to *n*-type GaAs. Platinum (Pt) is a commonly used Schottky metal for GaAs as it offers a near optimal Schottky barrier height compared to other suitable metals. Based on Myburg *et al.* findings, the barrier height parameter was set to 0.97 eV [27].

Table 3. Parameters Used to Module the ABC Schottky Solar Cell

Parameter	**Value**
Window Thickness	0.03 µm
Window Doping	8.8587×10^{16} cm^{-3}
Substrate Thickness	2.0789 µm
Substrate Doping	1×10^{16} cm^{-3}

The Silvaco ATLAS code that was used to model the cell shown in Figure 21 is found in Appendix F. The performance of the cell was evaluated using the slightly modified MATLAB code in Appendix B. The solar cell demonstrated an efficiency of 8.798% with a fill factor of 92.91. As shown in Figure 22, the solar cell has an I-V characteristic with a notably small open-circuit voltage.

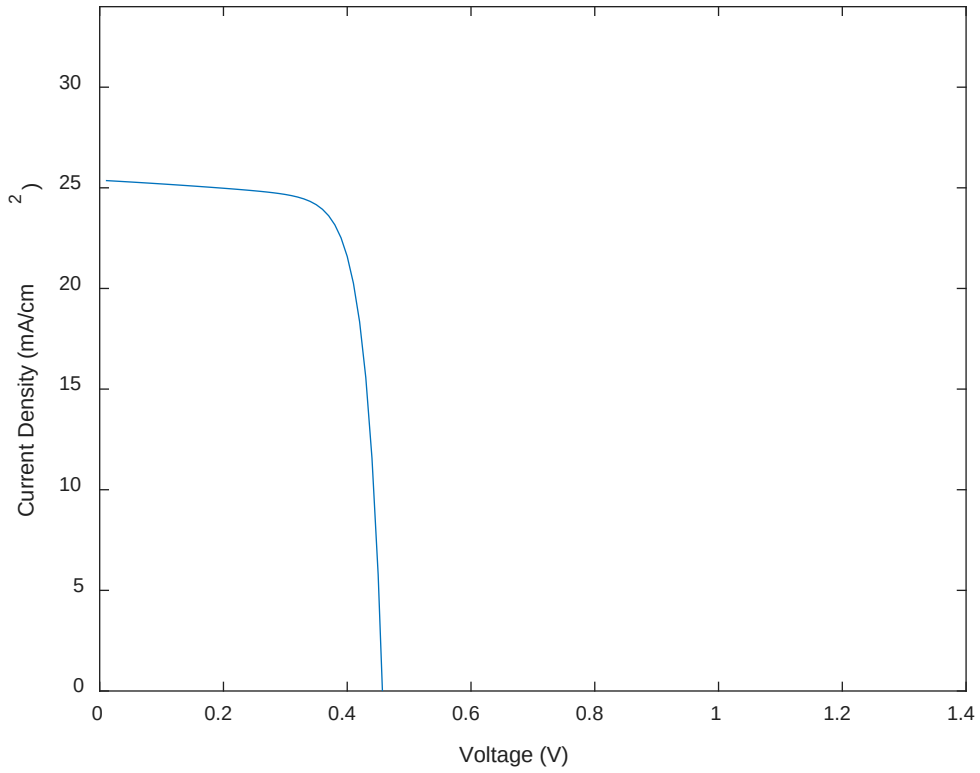

Figure 22. The I-V Characteristics of the ABC Schottky Solar Cell

The Schottky ABC solar cell demonstrated a relatively low efficiency of 8.787%, which would not be considered for commercial manufacturing. Interpreting Figure 22, we note that a significant factor for the drop in efficiency is the small built-in voltage. A low built-in voltage allows majority charge carriers to diffuse across the depletion region rather than provide current to the attached load. In this thesis, we evaluated three potential ways of increasing the built-in voltage in order to increase the solar cell efficiency.

The ideal process to increase the built-in voltage is from an organic interlayer that can be precisely placed between the Schottky metal and GaAs substrate. This allows for a significant reduction in manufacturing steps and complexity. Further manufacturing ease comes if this layer is screen printable. Campbell *et al.* demonstrated barrier height tuning of 1.0 eV with an organic layer while remarking it should be possible to shift it by substantially more [28]. Campbell accomplished this with organic layers between a Schottky metal and poly [2-methoxy, 5-(2'-ethyl-hexyloxy)-1,4-phenylene. Similarly, Gullu *et al*. doubled the Schottky barrier height of *n*-type Indium Phosphide (InP) with

DNA biopolymer nanofilms that were placed between the metal and semiconductor [29]. Gullu explained that the DNA molecule acts as a *p*-type semiconductor with a wide bandgap of 4.12 eV. Unfortunately, such a relationship has yet to be discovered for GaAs.

Another method to increase the effective barrier height is to grow an extremely thin *p*-doped emitter layer between the metal and semiconductor. Sassen *et al*. proposed introducing a highly dopped GaAs layer between the Schottky contact and the substrate [30]. This method when modeled does increase the effective barrier height as this is de facto forming a *p*-*n* junction. The growth of the highly doped emitter layer requires considerable energy, and surface etching is required to make room for the cathodes.

The third and chosen method to increase the effective barrier height is through low-energy ion-implantation. Wu *et al.* demonstrated a technique for enhancing the Schottky barrier height of *n*-type GaAs through ion-implantation of Arsenic (As) [31]. Wu goes on to state "the advantage of our method in which the near-surface stoichiometry is altered is that no *p*-type dopants need to be added to the GaAs to achieve barrier enhancement, and implantation also allows selective spatial alteration of the barrier height using conventional masking techniques." An ion-implanted Schottky ABC solar cell, shown in Figure 23, was modeled with the Silvaco ATLAS with code in Appendix G. The ion-implanted *p*-type emitter layer was set to a realistic doping concentration of 3×10^{19} cm^{-3}. The emitter layer was set to a realistic depth of 25 nm with a thickness of 2.0 nm.

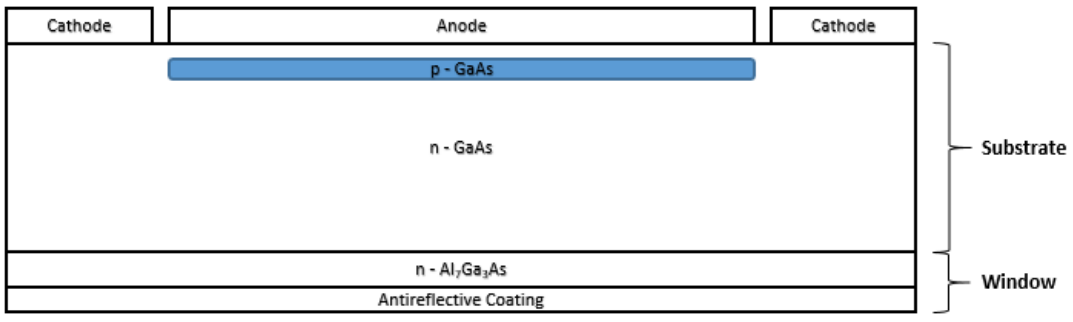

Figure 23. Schottky ABC PV Cell with a Zn Ion-Implanted Interlayer

The performance of the cell was evaluated using the slightly modified MATLAB code in Appendix B. The solar cell demonstrated efficiency was 13.42% with a fill factor of 93.68. As shown in Figure 24, the solar cell has an improved I-V characteristic with a larger open-circuit voltage.

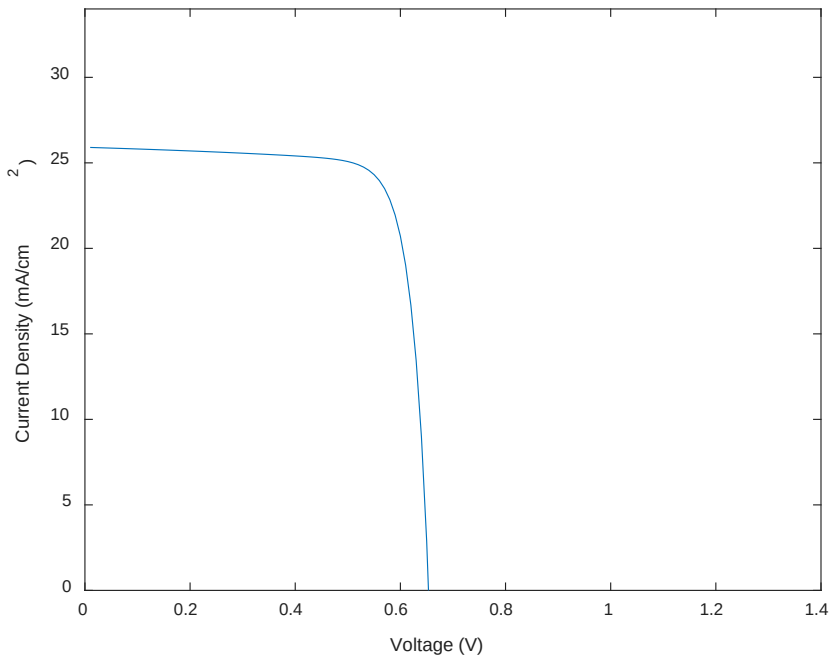

Figure 24. The I-V Characteristics of the Ion-Implanted ABC Schottky Solar Cell

The results shown in Figure 24 verify that by using ion-implantation the Schottky barrier height can be increased and, thus, efficiency improved. The manufacturing process for such a solar cell is shown in Figure [25].

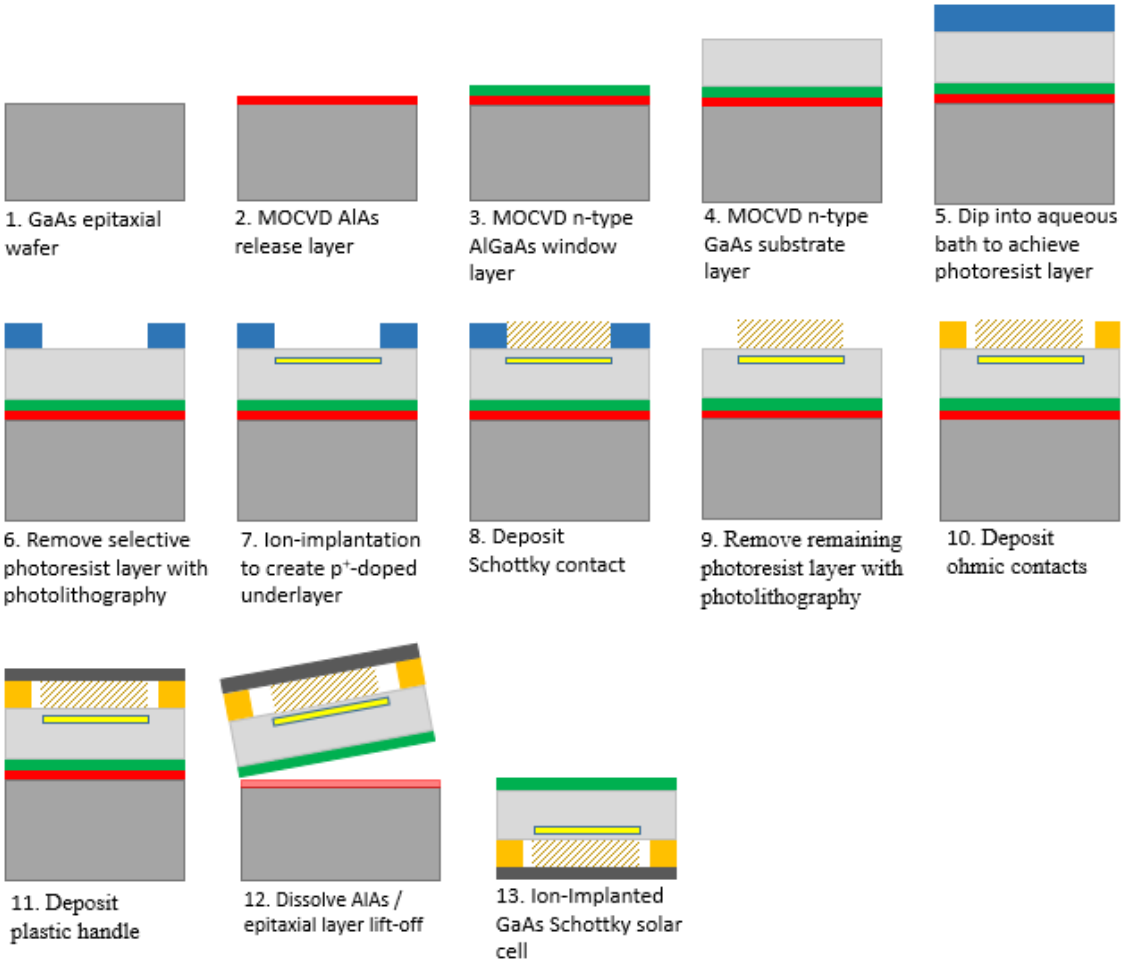

Figure 25. Envisioned Manufacturing Process for a Schottky ABC Solar Cell with an Ion-Implanted Emitter Layer

Wu's proposed method of ion-implanting Arsenic is limited to a *p*-type doping concentration of 1×10^{16} cm^{-3}; whereas, Stichtenoth *et al.* proposed instead to ion-implant Zinc (Zn) to a GaAs substrate layer [32]. As shown in Figure 26, a Zn ion-implanted emitter layer concentration of 3×10^{19} cm^{-3} with a depth of 25.0 nm is achievable. The thickness of the emitter layer was chosen to be 2.0 nm based Campbell's findings shown in Figure 27 [33].

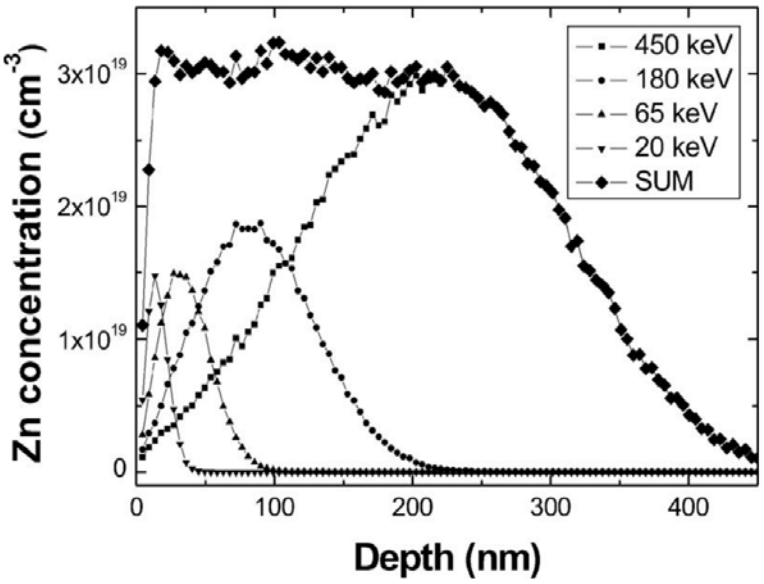

Figure 26. Depth vs. Concentration for Ion-Implanted Zn in GaAs Substrate. Source: [32].

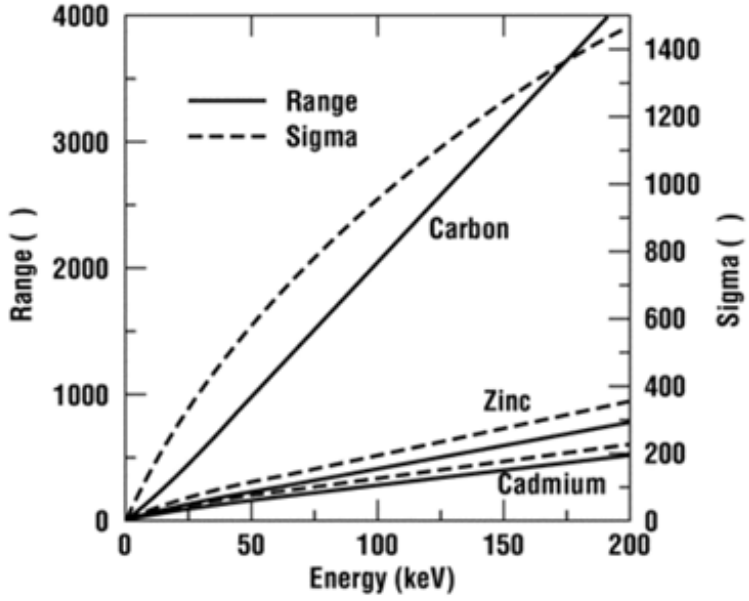

Figure 27. Relationship between *p*-type Dopants and GaAs. Source: [33].

IV. CONCLUSIONS

A. SUMMARY

In this thesis Silvaco ATLAS and MATLAB were used to design, model, and optimize several advanced solar cells. First, Alta Devices commercially available GaAs solar cell was modeled, which served the purpose of justifying our modeling technique and simulation software. This cell was also used as a baseline to be compared to the other cells modeled in this thesis research. The next cell modeled was the ABC GaAs solar cell based on Alta Device's patented concept. Moving the electrodes to the back of the cell eliminated shadowing, which may increase cell efficiency. A total of 1200 simulations were run and evaluated to find a near optimal configuration for the ABC GaAs solar cell. The results showed an unexpected loss of efficiency that may be explained by Silvaco ATLAS not accounting for photon recycling.

To make the ABC GaAs solar cell more manufacturable and cost efficient, the highly concentrated *p*-doped layer was removed and replaced by a Pt Schottky contact. In turn, this replaces the diode mechanism from a *p*-*n* junction to a Schottky junction. The simulated Schottky ABC GaAs solar cell displayed a significant loss of efficiency which was largely due to the drop in the built-in voltage. To increase the Schottky built-in voltage, a highly doped *p*-type interlayer was formed by the ion-implantation of Zn. The ion-implanted Schottky ABC GaAs solar cell displayed an increased efficiency relative to Schottky ABC GaAs solar cell but still with a much lower efficiency than the modeled *p*-*n* junction solar cells. Due to the reduction in production cost evident by replacing the highly-doped emitter layer in a *p*-*n* junction with an ion-implanted Schottky junction, the cell may warrant further research or production.

B. FUTURE WORK

1. Screen Printable Interlayer

Research indicated that thin layers can be placed between some substrates and Schottky contacts to increase the effective barrier height; however, such a relationship has yet to be discovered for GaAs. If such a relationship is discovered, it could greatly reduce

the manufacturing process for a Schottky ABC GaAs solar cell. Further reduction in the manufacturing process will be realized if the interlayer was screen printable

2. Photon Recycling

An electron-hole pair lost to radiative recombination has the potential to generate a new electron-hole pair within the semiconductor device due to the emitted photon. The likelihood is higher for such an occurrence in GaAs as compared to silicon due to its direct bandgap property. Silvaco ATLAS does not have a built-in method to account for photon recycling. A non-trivial fix has been identified for other similar semiconductor modeling software. If a method was established for Silvaco ATLAS to account for photon recycling, this would allow for more accurate modeling of solar cells.

3. Fabrication

In this thesis, we proposed a manufacturable method to fabricate a novel solar cell. Actual fabrication of said Zn ion-implanted Schottky ABC solar cell either in-house or at an external fabrication facility is possible with funding. A physical model would serve as a way to compare results to Silvaco ATLAS.

APPENDIX A. SILVACO ATLAS CODE FOR BASELINE FRONT CONTACT SOLAR CELL

```
go atlas simflags="-P 8"
set count= 1
set windowthick= 0.01
set windowdopconc= 1E20
set bulkthick= 3
set bulkdopconc= 1E16
set emitterthick= 0.3
set emitterdopconc= 1E16
set contactthick= 0.004
set totalbackthick= $contactthick+$emitterthick
set length= 1
set contactwidth=.15
set oxidewidth=1
set width=2*$oxidewidth+$contactwidth
##########
#Meshes
##########
mesh width=$length space.mult=1
x.mesh loc=0.0 s=$oxidewidth/20
x.mesh loc=$oxidewidth s=$contactwidth/60
x.mesh loc=$oxidewidth+$contactwidth s=$contactwidth/60
x.mesh loc=2*$oxidewidth+$contactwidth s=$oxidewidth/20
y.mesh loc=0.0 spac=$windowthick/40
y.mesh loc=$windowthick spac=$bulkthick/200
y.mesh loc=$windowthick+$bulkthick spac=$bulkthick/20
y.mesh loc=$windowthick+$bulkthick+$emitterthick spac=$emitterthick/20
region num=1 name=AlGaAs material=AlGaAs x.comp=.3 x.min=0.0 \
        x.max=$width y.min=0 y.max=$windowthick
region num=2 name=GaAs material=GaAs y.min=$windowthick \
        y.max=$windowthick+$bulkthick
region num=3 name=AlGas material=AlGaAs x.comp=.7 \
        y.min=$windowthick+$bulkthick \
        y.max=$windowthick+$bulkthick+$emitterthick
electrode num=1 name=cathode x.min=$oxidewidth \
        x.max=$oxidewidth+$contactwidth y.min=0.0 y.max=$contactthick
electrode num=2 name=anode bottom
doping region=1 uniform n.type conc=$windowdopconc y.min=0.0 y.max=$windowthick
doping region=2 uniform p.type conc=$bulkdopconc y.min=$windowthick \
        y.max=$windowthick+$bulkthick
doping region=3 uniform p.type conc=$emitterdopconc \
        y.min=$windowthick+$bulkthick \
```

```
        y.max=$windowthick+$bulkthick+$emitterthick
Contact name=anode resistance=1.3E8
interface optical reflect=0 p1.x=0 p2.x=$width p1.y=0.0 p2.y=0.0
######################
## MATERIAL PROPERTIES
######################
material material=GaAs AUGN=7e-30 AUGP=7e-30 COPT=1.3e-10 \
        TAUN=510e-09 TAUP=510e-09
######################
## Initialization
######################
models SRH OPTR CONMOB AUGER BGN temp=300 print
method newton itlimit=40
output con.band val.band opt.intens j.drift j.diffusion
solve init
######################
## Illuminated FWD Bias
######################  METAL.REFLECT
beam num=1 am1.5 x.o=$width/2 y.o=-1.5 angle=90 \
        wavel.start=0.200 wavel.end=2.5 wavel.num=200 verbose \
        BACK.REFL reflect=1
solve b1=0.01
solve b1=0.1
solve b1=0.5
solve b1=1.0
log outfile=AltaDevicesRecordEffCell_'$count'.log
solve vstep=0.01 vfinal=1.3 name=anode
log off
quit
```

APPENDIX B. MATLAB CODE FOR EVALUATING A SINGLE SOLAR CELL DESIGN

```
clear all;close all;
myarea = 3.5 * 1 * (1/(1E4))^2;
filename = 'BBB_Schottky_1.log'; delimiterIn = ' '; headerlinesIn = 20;
A1 = importdata(filename,delimiterIn,headerlinesIn);
plot(A1.data(:,15),A1.data(:,14)./myarea.*1E3)
axis([0 1.4 0 34])
xlabel('Voltage (V)'), ylabel('Current Density(mA)');
%% Efficiency
A1_power = A1.data(:,15).*A1.data(:,14);
A1_Percent_Efficiency = max(A1_power)/(A1.data(1,1)*myarea)*100
%% Fill Factor
areaundercurve = sum(A1.data(find(A1.data(:,14)>0),14).*0.01);
isc = A1.data(1,14);
voc = A1.data(find(A1.data(:,14)>0),16);
FF = areaundercurve/(isc*voc(end))
```

THIS PAGE INTENTIONALLY LEFT BLANK

APPENDIX C. MATLAB CODE TO CALL SILVACO ATLAS TO SIMULATE MULTIPLE DESIGNS

```
%clear all; uiimport('AltaDevicePatent_Bulk.in'); %copy and paste
directly into command line; save as a string.
S = AltaDevicePatentBulk;
BulkThickness = linspace(.5,3.5,20);
BulkDoping = logspace(16,19,20);
count=1;
for j=1:numel(BulkThickness)
     S(5,3) = {BulkThickness(j)};
    for k=1:numel(BulkDoping)
        S(6,3) = {BulkDoping(k)};
        S(2,3)= count;
        fileID =
fopen('C:\Users\FlavaFlave\Documents\MATLAB\Bulk\bulkworkingfile.in','w
');
            for i=1:length(S(:,1))
            fprintf(fileID, '%s ',S(i,:)');
            fprintf(fileID,'\n');
        end
        fclose(fileID);
        system("C:\sedatools\exe\deckbuild.exe -run
C:\Users\FlavaFlave\Documents\MATLAB\Bulk\bulkworkingfile.in")
        count=count+1;
    end
end
```

THIS PAGE INTENTIONALLY LEFT BLANK

APPENDIX D. SILVACO ATLAS CODE FOR ABC SOLAR CELL

```
go atlas simflags="-P 4"
set count= 1
set windowthick= 0.02
set windowdopconc= 1E16
set bulkthick= 3
set bulkdopconc= 1E17
set emitterthick= .3
set emitterdopconc= 1E19
set contactthick= 0.1
set totalbackthick= $contactthick+$emitterthick
set length= 1
set contactwidth=.5
set oxidewidth=.1
set emitterwidth=.9
set width= 3*$contactwidth+2*$oxidewidth+2*$emitterwidth
##########
#Meshes
##########
mesh width=$length space.mult=1
x.m loc=0.0 s=$width/25
x.m loc=$contactwidth s=$width/150
x.m loc=$contactwidth+$oxidewidth s=$width/150
x.m loc=$contactwidth+$oxidewidth+$emitterwidth s=$width/25
x.m loc=2*$contactwidth+$oxidewidth+$emitterwidth s=$width/25
x.m loc=2*$contactwidth+$oxidewidth+2*$emitterwidth s=$width/150
x.m loc=2*$contactwidth+2*$oxidewidth+2*$emitterwidth s=$width/150
x.m loc=3*$contactwidth+2*$oxidewidth+2*$emitterwidth s=$width/25
y.mesh loc=0.0 spac=$bulkthick/100
y.mesh loc=$windowthick spac=$bulkthick/100
y.mesh loc=$windowthick+$bulkthick spac=$bulkthick/150
y.mesh loc=$windowthick+$bulkthick+$emitterthick spac=$bulkthick/100
y.mesh loc=$windowthick+$bulkthick+$emitterthick+$contactthick spac=$bulkthick/100
region num=1 name=AlGaAs material=AlGaAs x.comp=.7 y.min=0.0 \
        y.max=$windowthick
region num=2 name=GaAs material=GaAs y.min=$windowthick \
        y.max=$windowthick+$bulkthick
region num=3 name=Vacuum material=Vacuum y.min=$windowthick+$bulkthick \
        y.max=$windowthick+$bulkthick+$totalbackthick
region num=4 name=AlGas material=AlGaAs x.comp=.3 \
        y.min=$windowthick+$bulkthick \
        y.max=$windowthick+$bulkthick+$emitterthick \
        x.min=$contactwidth+$oxidewidth \
```

```
        x.max=2*$contactwidth+$oxidewidth+2*$emitterwidth
electrode num=1 name=cathode y.min=$windowthick+$bulkthick \
        y.max=$windowthick+$bulkthick+$contactthick x.min=0 x.max=$contactwidth
electrode num=2 name=anode y.min=$windowthick+$bulkthick+$emitterthick \
        y.max=$windowthick+$bulkthick+$emitterthick+$contactthick \
        x.min=$contactwidth+$oxidewidth+$emitterwidth \
        x.max=2*$contactwidth+$oxidewidth+$emitterwidth
electrode num=3 name=cathode y.min=$windowthick+$bulkthick \
        y.max=$windowthick+$bulkthick+$contactthick \
        x.min=2*$contactwidth+2*$oxidewidth+2*$emitterwidth \
        x.max=3*$contactwidth+2*$oxidewidth+2*$emitterwidth
doping region=1 uniform n.type conc=$windowdopconc y.min=0.0 y.max=$windowthick
doping region=2 uniform n.type conc=$bulkdopconc y.min=$windowthick \
        y.max=$windowthick+$bulkthick
doping region=4 uniform p.type conc=$emitterdopconc \
        y.min=$windowthick+$bulkthick \
        y.max=$windowthick+$bulkthick+$emitterthick
interface optical reflect=0 p1.x=0 p2.x=$width p1.y=0.0 p2.y=0.0
interface optical reflect=1 \
        p1.x=$contactwidth+$oxidewidth \
        p2.x=$contactwidth+$oxidewidth+$emitterwidth \
        p1.y=$windowthick+$bulkthick+$emitterthick \
        p2.y=$windowthick+$bulkthick+$emitterthick+$contactthick
interface optical reflect=1 \
        p1.x=$contactwidth+$oxidewidth+$emitterwidth+$contactwidth \
        p2.x=$contactwidth+$oxidewidth+$emitterwidth+$contactwidth+$emitterwidth \
        p1.y=$windowthick+$bulkthick+$emitterthick \
        p2.y=$windowthick+$bulkthick+$emitterthick+$contactthick
######################
## Material Properties
######################
material material=GaAs AUGN=7e-30 AUGP=7e-30 COPT=1.3e-10 \
        TAUN=510e-09 TAUP=510e-09
######################
## Initialization
######################
models SRH OPTR CONMOB AUGER BGN temp=300 print
method newton
output con.band val.band opt.intens j.drift j.diffusion
solve init
######################
## Illuminated FWD Bias
######################
beam num=1 am1.5 x.o=$width/2 y.o=-1.5 angle=90 \
        wavel.start=0.200 wavel.end=2.5 wavel.num=200 verbose \
```

```
        metal.reflect reflect=1
solve b1=1.0
log outfile=Baseline_'$count'.log
solve vstep=0.01 vfinal=1.2 name=anode
log off
quit
```

THIS PAGE INTENTIONALLY LEFT BLANK

APPENDIX E. MATLAB CODE FOR EVALUATING MULTIPLE SOLAR CELL DESIGNS

```
totalnumberfiles = 400;
mydata= cell(1, totalnumberfiles);
myarea = 3.5 * 1 * (1/(1E4))^2 ;
for k = 1:totalnumberfiles
  filename = sprintf('ABC_Solar_Cell_Bulk_%d.log', k); delimiterIn = '
'; headerlinesIn = 20;
  FileNum{k} = importdata(filename,delimiterIn,headerlinesIn);
  Power{k} = FileNum{k}.data(:,16).*FileNum{k}.data(:,14);
  Efficiency{k} = max(Power{k})/(FileNum{k}.data(1,1)*myarea);
end
EmitterThickness = linspace(.1,2,20);
EmitterDoping = logspace(17,20,20);
Eff = cell2mat(Efficiency);
EffMatrix = zeros(numel(EmitterThickness),numel(EmitterDoping));
ph=1;
for l=1:numel(EmitterThickness)
    for m=1:numel(EmitterDoping)
        EffMatrix(l,m)=Eff(ph);
        ph=ph+1;
    end

end
surf((EmitterDoping),EmitterThickness,EffMatrix)
set(gca, 'XScale','log')
xlabel('Doping (cm^{-3})'), ylabel('Thickness (\mum)'),
zlabel('Efficiency');
[Ix,Iy]=find(EffMatrix==max(max(EffMatrix)));
EmitterDoping(Iy)
EmitterThickness(Ix)
max(max(EffMatrix))
%% Fill Factor
areaundercurve =
sum(FileNum{Ix*Iy}.data(find(FileNum{Ix*Iy}.data(:,14)>0),14).*0.01);
isc = FileNum{Ix*Iy}.data(1,14);
voc = FileNum{Ix*Iy}.data(find(FileNum{Ix*Iy}.data(:,14)>0),16);
FF = areaundercurve/(isc*voc(end))
```

THIS PAGE INTENTIONALLY LEFT BLANK

APPENDIX F. SILVACO ATLAS CODE FOR A SCHOTTKY ABC SOLAR CELL

```
go atlas simflags="-P 4"
set count= 1
set windowthick= 0.03
set windowdopconc= 8.8587E16
set bulkthick= 2.0789
set bulkdopconc= 1E16
set contactthick= 0.1
set length= 1
set cathodewidth= 0.25
set anodewidth= 2.5
set oxidewidth= 0.25
set width= 2*$cathodewidth+$anodewidth+2*$oxidewidth
##########
#Meshes
##########
mesh width=$length space.mult=1
x.m loc=0.0 s=$cathodewidth/10
x.m loc=$cathodewidth s=$cathodewidth/15
x.m loc=$cathodewidth+$oxidewidth s=$oxidewidth/15
x.m loc=$cathodewidth+$oxidewidth+$anodewidth/2  s=$oxidewidth/2
x.m loc=$cathodewidth+$oxidewidth+$anodewidth s=$oxidewidth/15
x.m loc=$cathodewidth+2*$oxidewidth+$anodewidth s=$cathodewidth/15
x.m loc=2*$cathodewidth+2*$oxidewidth+$anodewidth s=$cathodewidth/10
y.mesh loc=0.0 spac=$windowthick/5
y.mesh loc=$windowthick spac=$windowthick/5
y.mesh loc=2*$windowthick spac=$windowthick/5
y.mesh loc=$windowthick+$bulkthick/2 spac=$bulkthick/5
y.mesh loc=$windowthick+$bulkthick spac=$bulkthick/500
y.mesh loc=$windowthick+$bulkthick+$contactthick spac=$contactthick/5
y.mesh loc=$windowthick+$bulkthick+$contactthick spac=$contactthick/5
region num=1 name=AlGaAs material=AlGaAs x.comp=.7 y.min=0.0 \
        y.max=$windowthick
region num=2 name=GaAs material=GaAs y.min=$windowthick \
        y.max=$windowthick+$bulkthick
region num=3 name=Vacuum material=Vacuum y.min=$windowthick+$bulkthick \
        y.max=$windowthick+$bulkthick+$contactthick
electrode num=1 name=cathode y.min=$windowthick+$bulkthick \
        y.max=$windowthick+$bulkthick+$contactthick \
        x.min=0 x.max=$cathodewidth
electrode num=2 name=anode y.min=$windowthick+$bulkthick \
        y.max=$windowthick+$bulkthick+$contactthick \
```

```
        x.min=$cathodewidth+$oxidewidth \
        x.max=$cathodewidth+$oxidewidth+$anodewidth
electrode num=3 name=cathode y.min=$windowthick+$bulkthick \
        y.max=$windowthick+$bulkthick+$contactthick \
        x.min=$cathodewidth+2*$oxidewidth+$anodewidth \
        x.max=2*$cathodewidth+2*$oxidewidth+$anodewidth
doping region=1 uniform n.type conc=$windowdopconc \
        y.min=0.0 y.max=$windowthick
doping region=2 uniform n.type conc=$bulkdopconc y.min=$windowthick \
        y.max=$windowthick+$bulkthick
contact name=anode workf=4.07+0.97
interface optical reflect=0 p1.x=0 p2.x=$width p1.y=0.0 p2.y=0.0
######################
## Material Properties
######################
material material=GaAs  AUGN=7e-30 AUGP=7e-30 COPT=1.3e-10 \
        TAUN=510e-09 TAUP=510e-09
######################
## Initialization
######################
models SRH OPTR CONMOB AUGER BGN temp=300 print
method newton
output con.band val.band opt.intens j.drift j.diffusion
solve init
######################
## Illuminated FWD Bias
######################
beam num=1 am1.5 x.o=$width/2 y.o=-1.5 angle=90 \
        wavel.start=0.200 wavel.end=2.5 wavel.num=200 verbose \
        metal.reflect reflect=1
solve b1=1.0
log outfile=Schottky_'$count'.log
solve vstep=0.01 vfinal=1.2 name=anode
log off
quit
```

APPENDIX G. SILVACO ATLAS CODE FOR A ZINC ION-IMPLANTED SCHOTTKY ABC SOLAR CELL

```
go atlas simflags="-P 4"
set count= 1
set windowthick= 0.03
set windowdopconc= 8.8587E16
set bulkthick= 2.0789
set bulkdopconc= 1E16
set implantthick= 0.002
set implantdopconc= 3E19
set intermediatethick= 0.025
set cathodethick= 0.1
set anodethick=0.1
set length= 1
set cathodewidth= 0.25
set anodewidth= 2.5
set oxidewidth= 0.25
set width= 2*$cathodewidth+$anodewidth+2*$oxidewidth
##########
#Meshes
##########
mesh width=$length space.mult=1
x.m loc=0.0 s=$cathodewidth/10
x.m loc=$cathodewidth s=$cathodewidth/15
x.m loc=$cathodewidth+$oxidewidth s=$oxidewidth/15
x.m loc=$cathodewidth+$oxidewidth+$anodewidth/2  s=$oxidewidth/2
x.m loc=$cathodewidth+$oxidewidth+$anodewidth s=$oxidewidth/15
x.m loc=$cathodewidth+2*$oxidewidth+$anodewidth s=$cathodewidth/15
x.m loc=2*$cathodewidth+2*$oxidewidth+$anodewidth s=$cathodewidth/10
y.mesh loc=0.0 spac=$windowthick/5
y.mesh loc=$windowthick spac=$windowthick/5
y.mesh loc=2*$windowthick spac=$windowthick/5
y.mesh loc=$windowthick+$bulkthick/2 spac=$bulkthick/5
y.mesh loc=$windowthick+$bulkthick-2*$implantthick-$intermediatethick \
        spac=$implantthick/50
y.mesh loc=$windowthick+$bulkthick-$implantthick-$intermediatethick \
        spac=$implantthick/50
y.mesh loc=$windowthick+$bulkthick-$intermediatethick spac=$intermediatethick/50
y.mesh loc=$windowthick+$bulkthick spac=$intermediatethick/50
y.mesh loc=$windowthick+$bulkthick+$anodethick spac=$anodethick/2
y.mesh loc=$windowthick+$bulkthick+$cathodethick spac=$cathodethick/2
region num=1 name=AlGaAs material=AlGaAs x.comp=.7 \
        y.min=0.0 y.max=$windowthick
```

```
region num=2 name=GaAs material=GaAs y.min=$windowthick \
        y.max=$windowthick+$bulkthick x.min=0 x.max=$cathodewidth+$oxidewidth
region num=3 name=GaAs material=GaAs y.min=$windowthick \
        y.max=$windowthick+$bulkthick-$implantthick-$intermediatethick \
        x.min=$cathodewidth+$oxidewidth \
        x.max=$cathodewidth+$oxidewidth+$anodewidth
region num=4 name=GaAs material=GaAs \
        y.min=$windowthick+$bulkthick-$implantthick-$intermediatethick \
        y.max=$windowthick+$bulkthick-$intermediatethick \
        x.min=$cathodewidth+$oxidewidth \
        x.max=$cathodewidth+$oxidewidth+$anodewidth
region num=5 name=GaAs material=GaAs \
        y.min=$windowthick+$bulkthick-$intermediatethick \
        y.max=$windowthick+$bulkthick \
        x.min=$cathodewidth+$oxidewidth \
        x.max=$cathodewidth+$oxidewidth+$anodewidth
region num=6 name=GaAs material=GaAs y.min=$windowthick \
        y.max=$windowthick+$bulkthick \
        x.min=$cathodewidth+$oxidewidth+$anodewidth \
        x.max=2*$cathodewidth+2*$oxidewidth+$anodewidth
region num=7 name=Vacuum material=Vacuum y.min=$windowthick+$bulkthick \
        y.max=$windowthick+$bulkthick+$cathodethick \
        x.min=$cathodewidth x.max=$cathodewidth+$oxidewidth
region num=8 name=Vacuum material=Vacuum y.min=$windowthick+$bulkthick \
        y.max=$windowthick+$bulkthick+$cathodethick \
        x.min=$cathodewidth+$oxidewidth+$anodewidth \
        x.max=$cathodewidth+2*$oxidewidth+$anodewidth
electrode num=1 name=cathode y.min=$windowthick+$bulkthick \
        y.max=$windowthick+$bulkthick+$cathodethick \
        x.min=0 x.max=$cathodewidth
electrode num=2 name=anode y.min=$windowthick+$bulkthick \
        y.max=$windowthick+$bulkthick+$cathodethick \
        x.min=$cathodewidth+$oxidewidth \
        x.max=$cathodewidth+$oxidewidth+$anodewidth
electrode num=3 name=cathode y.min=$windowthick+$bulkthick \
        y.max=$windowthick+$bulkthick+$cathodethick \
        x.min=$cathodewidth+2*$oxidewidth+$anodewidth \
        x.max=2*$cathodewidth+2*$oxidewidth+$anodewidth
doping region=1 uniform n.type conc=$windowdopconc y.min=0.0 y.max=$windowthick
doping region=2 uniform n.type conc=$bulkdopconc y.min=$windowthick \
        y.max=$windowthick+$bulkthick x.min=0 x.max=$cathodewidth+$oxidewidth
doping region=3 uniform n.type conc=$bulkdopconc y.min=$windowthick \
        y.max=$windowthick+$bulkthick-$implantthick-$intermediatethick \
        x.min=$cathodewidth+$oxidewidth \
        x.max=$cathodewidth+$oxidewidth+$anodewidth
```

```
doping region=4 uniform p.type conc=$implantdopconc \
        y.min=$windowthick+$bulkthick-$implantthick-$intermediatethick \
        y.max=$windowthick+$bulkthick-$intermediatethick \
        x.min=$cathodewidth+$oxidewidth \
        x.max=$cathodewidth+$oxidewidth+$anodewidth
doping region=5 uniform n.type conc=$bulkdopconc \
        y.min=$windowthick+$bulkthick-$intermediatethick \
        y.max=$windowthick+$bulkthick \
        x.min=$cathodewidth+$oxidewidth \
        x.max=$cathodewidth+$oxidewidth+$anodewidth
doping region=6 uniform n.type conc=$bulkdopconc y.min=$windowthick \
        y.max=$windowthick+$bulkthick \
        x.min=$cathodewidth+$oxidewidth+$anodewidth \
        x.max=2*$cathodewidth+2*$oxidewidth+$anodewidth
contact name=anode workf=4.07+0.97
interface optical reflect=0 p1.x=0 p2.x=$width p1.y=0.0 p2.y=0.0
######################
## Material Properties
######################
material material=GaAs AUGN=7e-30 AUGP=7e-30 COPT=1.3e-10 \
        TAUN=510e-09 TAUP=510e-09
######################
## Initialization
######################
models SRH OPTR CONMOB AUGER BGN temp=300 print
method newton
output con.band val.band opt.intens j.drift j.diffusion
solve init
######################
## Illuminated FWD Bias
######################
beam num=1 am1.5 x.o=$width/2 y.o=-1.5 angle=90 \
        wavel.start=0.200 wavel.end=2.5 wavel.num=200 verbose \
        metal.reflect reflect=1
solve b1=1.0
log outfile=IonImplanted_Schottky_'$count'.log
solve vstep=0.01 vfinal=1.2 name=anode
log off

        quit
```

THIS PAGE INTENTIONALLY LEFT BLANK

LIST OF REFERENCES

[1] Fraunhofer Institute for Solar Energy Systems. (2016, Nov. 17). Photovoltaics report. Accessed May 23, 2018. [Online]. Available: ,https://www.ise.fraunhofer.de/content/dam/ise/de/documents/publications/studies/Photovoltaics-Report.pdf

[2] M. A. Green. (2002, Aug. 6). Photovoltaics: Coming of age. Accessed May 23 2018. [Online]. Available: http://ieeexplore.ieee.org/stamp/stamp.jsp?tp=&arnumber=111582

[3] National Renewable Energy Laboratory. (2016, Dec. 2). Best research-cell efficiencies. Accessed May 23, 2018. [Online]. Available: https://www.nrel.gov/pv/assets/images/efficiency-chart.png

[4] P. Michalopoulos, "A novel approach for the development and optimization of state-of-the-art photovoltaic devices using Silvaco," M.S. thesis, Dept. of Elec. and Comp. Engr., Naval Postgraduate School, Monterey, CA, USA, 2002.

[5] K. Fotis, "Modeling and simulation of a dual-junction CIGS solar cell using Silvaco ATLAS," M.S. thesis, Dept. of Elec. and Comp. Engr., Naval Postgraduate School, Monterey, CA, USA, 2012.

[6] D. Columbus, "Design and optimization of copper indium gallium selenide solar cells for lightweight battlefield application," M.S. thesis, Dept. of Elec. and Comp. Engr., Naval Postgraduate School, Monterey, CA, USA, 2014.

[7] S. Green, "Interdigitated back-surface-contact solar cell modeling using Silvaco Atlas," M.S. thesis, Dept. of Elec. and Comp. Engr., Naval Postgraduate School, Monterey, CA, USA, 2015.

[8] D. Katzman, "Design and optimization of copper indium gallium selenide thin film solar cells," M.S. thesis, Dept. of Elec. and Comp. Engr., Naval Postgraduate School, Monterey, CA, USA, 2015.

[9] J. O'Connor, "Design and simulation of novel, high-efficiency, back-contact solar cells," M.S. dissertation, Dept. of Elec. and Comp. Engr., Naval Postgraduate School, Monterey, CA, USA, 2017.

[10] S. Sze, *Physics of Semiconductor Devices*, 1st Ed. New York, NY, USA: John Wiley & Sons, 1969.

[11] J. Lindmayer and C. Wrigley, *Fundamentals of Semiconductor Devices*, 1st Ed. New York, NY, USA: Van Nostrand Reinhold Company, 1965.

[12] "Solar energy," class notes for EC3240: Renewable Energy at Miliatry Bases and for the Warfighter, Dept. of Elec. and Comp. Engr., Naval Postgraduate School, Monterey, CA, USA, 2017.

[13] TU Delft University. (n.d.). Solar cells. Accessed May 15, 2018. [Online]. Available: https://ocw.tudelft.nl/courses/solar-cells/

[14] A. Luque and S. Hegedus, *Handbook of Photovoltaic Science and Engineering*, 1st Ed. Chichester, England: John Wiley & Sons Inc., 2003.

[15] C. Hu and R. White, *Solar Cells from Basics to Advanced Systems*, 1st Ed. New York, NY, USA: McGraw-Hill Book Company, 1983.

[16] R. Kilway, "Five-junction solar cell optimization using Silvaco Atlas," M.S. thesis, Dept. of Elec. and Comp. Engr., Naval Postgraduate School, Monterey, CA, USA, 2017.

[17] S. Gupta, N. Ghosh, and A. Banerjee, *Wave Optics: Basic Concepts and Contemporary Trends*, 1st Ed. Boca Raton, FL, USA: CRC Press, 2016.

[18] *Atlas User's Manual—Device Simulation Software*, Silvaco, Inc., Santa Clara, CA, USA, 2016.

[19] P. Campbell and M. Green, "Light trapping properties of pyramidally textured surfaces," *J. of Applied Physics*, vol. 62, no. 243, 1987.

[20] X. Wang, M. Khan, J. Gray, M. Alam, and M. Lundstrom, "Design of GaAs solar cells operating close to the Shockley-Queisser Limit," *IEEE Journal of Photovoltaics*, vol. 3, no. 2, 2013.

[21] G. Hooft, "The radiative recombination coefficient of GaAs from laser delay measurements and effective nonradiative carrier lifetimes," *Applied Physics Letters*, vol. 39, no. 389, 1981.

[22] Alta Devices. (n.d.). "Alta Devices brochure." Accessed May 9, 2018. [Online]. Available: https://www.altadevices.com/wp-content/uploads/2018/04/Alta-Corporate-Brochure.pdf

[23] G. Letay, M. Hermle, and A. Bett, "Simulating single-junction GaAs solar cells including photon recycling," *Prog. Photovolt: Res. Appl*., vol. 14, pp. 683–696, 2006.

[24] A. Walker, O. Hohn, D. Micha, B. Blasi, A. Bett, and F. Dimroth, "Impact of photon recycling on GaAs solar cell designs," *IEEE Journal of Photovoltaics*, vol. 5, no. 6, 2015.

[25] I. Kizilyalli. “Photovoltaic Device,” U.S. Patent Grant US8895845B2, 23 Oct 2008.

[26] S. Byrnes. “Schottky junction solar cells.” Acessed May 30, 2018. [Online]. Available: https://sjbyrnes.com/NSE290-FinalPaper.pdf

[27] G. Myburg and F. Auret, “Influence of the electron beam evaporation rate of Pt and the semiconductor carrier density on the characteristics of Pt/n-GaAs Schottky contacts,” *Journal of Applied Physics*, vol. 71, no. 6172, 1992.

[28] I. Campbell, T. Zawodzinski, J. Kress, R. Martin, and D. Smith. “Controlling Schottky energy barriers in organic electronic devices using self-assembled monolayers,” *Physical Review B*, vol. 54, no. 20, 1996.

[29] O. Gullu. “Ultrahigh (100%) barrier modification of n-InP Schottky diode by DNA biopolymer nanofilms,” *Microelectronic Engineering*, vol. 87, pp. 648–651, 2010.

[30] S. Sassen, B. Witzigmann, C. Wolk, and H. Brugger. “Barrier height engineering on GaAs THz Schottky diodes by means of high-low doping, InGaAs- and InGaP-layers,” *IEEE Transactions on Electron Devices*, vol. 47, no. 1, 2000.

[31] C. Wu, C. Pai, S. Pearton, F. Ren, E. Lane, and D. Schleich. “Schottky barrier enhancement on n-type GaAs by As implantation,” *Phys. Stat. Sol.*, vol. 118, 1990.

[32] D. Stichtenoth, K. Wegener, C. Gutsche, I. Regolin, F. Tegude, W. Prost, M. Seibt, and C. Ronning. “P-type doping of GaAs nanowires,” *Appl. Phys. Lett.*, vol. 92, 2008.

[33] S. Campbell, *The Science and Engineering of Microelectronic Fabrication*, 2nd Ed. New York, NY, USA: Oxford University Press, 2001.

THIS PAGE INTENTIONALLY LEFT BLANK

INITIAL DISTRIBUTION LIST

1. Defense Technical Information Center
   Ft. Belvoir, Virginia

2. Dudley Knox Library
   Naval Postgraduate School
   Monterey, California